Larhyss Journal, ISSN 1112-3680, n°65, Mars 2026, pp. 193-285

Monograph

NORMAL FLOW DEPTH IN TRAPEZOIDAL CHANNELS A DARCY-WEISBACH-RMM SOLUTION FRAMEWORK

***ACHOUR B.*[1*], *AMARA L.*[2]**

[1] Professor, Research Laboratory in Subterranean and Surface Hydraulics (LARHYSS), University of Biskra, PO Box 145 RP, Biskra, Algeria
[2] Professor, Department of Civil Engineering and Hydraulics, Faculty of Science and Technology, University of Jijel, PO Box 98, Ouled Aissa, Jijel, Algeria

(*) bachir.achour@larhyss.net

Research Article – Available at http://larhyss.net/ojs/index.php/larhyss/index
Received June 12, 2025, Received in revised form February 17, 2026, Accepted February 20, 2026

ABSTRACT

This monograph establishes a mathematically rigorous framework for determining the normal flow depth in trapezoidal open channels by reformulating the problem within the Darcy-Weisbach-Rough Model Method (RMM) structure. Unlike classical Manning- or Chezy-based approaches, whose resistance parameters depend implicitly on the unknown flow depth, the proposed formulation yields a physically self-consistent, dimensionless implicit governing equation free from circular dependence.

The problem reduces to a nonlinear algebraic fixed-point equation in a reduced flow depth variable, expressed solely in terms of measurable quantities: relative conductivity, geometric parameters, slope, roughness, and viscosity.

The nonlinear fixed-point operator associated with the implicit governing equation satisfies a Lipschitz condition with constant strictly less than unity over the investigated hydraulic domain, i.e., conductivity varying within the range $0.1 \leq Q^* \leq 4$, and wall inclination angle such as $10° \leq \alpha \leq 80°$, thereby guaranteeing strong contraction, numerical stability, and rapid geometric convergence of the iterative solution.

Several solution strategies are derived and analytically examined, namely: an enhanced fixed-point iteration with an adaptive initial estimate (Initial guess), a controlled cube-root linearization producing an explicit closed-form approximation, an Aitken-Steffensen accelerated one-shot scheme obtained from finite-difference extrapolation, and Newton and secant corrections interpreted through local linearization theory.

Error behavior is analyzed through amplification properties of the nonlinear mapping, revealing a geometry-driven structure of deviation that is independent of the selected numerical strategy. Moderate sidewall inclinations, particularly around 45°, reduce the

geometric nonlinearity of the governing equation and enhance the contractive strength of the fixed-point operator; notably, the numerical deviations reach their minimum near this angle, indicating an optimal balance between hydraulic behavior and computational stability.

The results confirm that the implicit governing equation is globally well-conditioned and that appropriately constructed explicit or semi-explicit approximations achieve accuracy levels comparable to fully converged iterative solutions. The proposed framework therefore provides both theoretical clarity and computational efficiency for the normal-flow depth problem in trapezoidal channels.

Keywords: Normal flow depth; Trapezoidal channels; Darcy-Weisbach relationship; Rough Model Method (RMM); Fixed-point iteration; Approximate models, Adaptive initial guess; Convergence analysis; Explicit approximation.

INTRODUCTION

The determination of normal flow depth has historically constituted one of the fundamental and recurring challenges in open-channel hydraulics. In earlier practice, engineers relied predominantly on graphical tools, design charts, and tabulated solutions derived from resistance laws, as documented in classical references (Chow, 1973; French, 1986; Sinniger and Hager, 1989). These methods provided practical estimates but were inherently limited by interpolation accuracy and restricted parameter ranges. With the advancement of computational tools, the focus progressively shifted toward numerical procedures, particularly iterative root-finding strategies designed to solve the nonlinear uniform-flow equations more precisely. More recently, research efforts have extended further to develop closed-form or semi-explicit approximations intended to retain analytical clarity while reducing computational effort. This evolution reflects the continuing demand for solution techniques that balance hydraulic rigor, numerical reliability, and practical efficiency in engineering design.

A substantial body of research has sought to establish compact analytical formulations for the relative normal flow depth in trapezoidal channels, particularly through adaptations of the Manning and Chezy uniform-flow equations. Notable contributions include those of Swamee (1994), Swamee and Rathie (2004), Vatankhah (2013), and Amara and Achour (2023), among others, who derived implicit relationships intended to simplify practical computation. While these approaches have achieved wide acceptance in engineering applications due to their apparent simplicity and convenience, they rest on an underlying conceptual inconsistency when subjected to strict dimensionless analysis.

Specifically, both Manning's roughness coefficient n and Chezy's coefficient C are commonly introduced as fixed parameters characteristic of a given channel. However, theoretical analysis and empirical evidence demonstrate that these coefficients are not intrinsic constants; rather, they depend systematically on hydraulic variables such as flow depth, hydraulic radius, Reynolds number, and the relative roughness of the boundary. Consequently, their numerical values cannot be prescribed independently of the very flow

conditions they are meant to characterize. This interdependence introduces an implicit circularity into formulations that treat resistance coefficients as known inputs. The investigations of Achour and collaborators (Achour and Bedjaoui, 2006; Achour and Amara, 2020a; 2020b) explicitly clarified this dependency, showing that the resistance coefficient varies with the normal depth itself, thereby challenging the conceptual validity of dimensionless equations derived from Manning- or Chezy-based assumptions.

This situation gives rise to a fundamental conceptual inconsistency. The classical dimensionless relationships derived from Manning's or Chezy's equations implicitly presume that the resistance coefficient is specified independently and a priori, prior to determining the normal flow depth. In practice, however, the resistance coefficient is itself a function of hydraulic variables, notably flow depth, hydraulic radius, Reynolds number, and boundary roughness, which depend directly on the very normal depth being sought. Consequently, the computation becomes logically circular: the unknown depth is determined using a resistance parameter whose value cannot be established without already knowing that flow depth.

Any normal-flow depth expression constructed directly from Manning's or Chezy's formulation therefore embeds this internal dependence, effectively treating as constant a quantity that varies with the solution variable. Although such formulas may appear algebraically compact and computationally convenient, they lack strict physical self-consistency. Their apparent explicitness is, in fact, conditional upon an implicit assumption regarding hydraulic conditions that are not yet determined, thereby weakening the theoretical integrity of the resulting dimensionless representation.

In response to this inconsistency, subsequent investigations introduced a substantive methodological reorientation by replacing the Manning and Chezy formulations with the Darcy-Weisbach relationship integrated into the Rough Model Method (RMM) framework (Achour and Bedjaoui, 2006; Achour, 2014; Lakehal and Achour, 2014; Sehtal and Achour, 2023). This shift represents more than a change in resistance law; it constitutes a reformulation of the normal-flow depth problem on a physically coherent foundation. Within the Darcy-Weisbach-RMM framework, the friction factor is embedded in a rough reference model transformation, enabling it to be treated consistently without introducing circular dependence on the unknown flow depth.

As a result, the governing relationship for the relative normal flow depth can be derived as a fully self-contained, dimensionless implicit equation expressed solely in terms of measurable geometric and hydraulic quantities. Unlike Manning-based expressions, which implicitly rely on a resistance parameter varying with flow depth, the RMM formulation removes any reliance on empirically prescribed, condition-dependent coefficients. In doing so, it restores physical consistency to the uniform-flow analysis and establishes a rigorous theoretical platform from which both stable numerical procedures and accurate explicit approximations can be developed.

Accordingly, the principal objective of the present study is to develop a computational framework for determining normal flow depth in trapezoidal open channels that is at once operationally practical, numerically accurate, and physically self-consistent. The

approach is specifically designed to eliminate the conceptual and methodological limitations inherent in formulations that treat resistance coefficients as prescribed constants, despite their well-established dependence on hydraulic state variables and the very normal flow depth being sought.

In trapezoidal channels, the normal flow depth is a governing design parameter: it controls discharge capacity, influences energy slope and wetted perimeter, and sets the reference condition for gradually varied flow analysis. A robust computational strategy must therefore remain reliable across broad ranges of relative conductivity, sidewall inclination, and boundary roughness, while relying exclusively on parameters that can be directly measured or specified with engineering confidence. The methodology advanced in this study addresses these requirements by ensuring mathematical closure of the governing relationship and by maintaining numerical stability under diverse geometric and hydraulic conditions.

To achieve this objective, the study intentionally adopts the Darcy-Weisbach equation in conjunction with the Rough Model Method (RMM) as the fundamental modeling framework. This selection represents a deliberate methodological repositioning rather than a simple substitution of one resistance law for another. Its purpose is to remove the inherent circularity associated with flow depth-dependent empirical coefficients and to establish a mathematically closed formulation in which the governing relationship does not presuppose the value of a resistance parameter that depends on the unknown solution.

Within the Darcy-Weisbach-RMM framework, the uniform-flow problem is reformulated entirely in terms of measurable geometric and hydraulic quantities, and the resistance effects are consistently embedded in the rough reference model transformation. The resulting development leads to a fully self-contained, dimensionless implicit equation governing a reduced normal-flow depth variable. This equation constitutes the central analytical structure of the study, providing a rigorous mathematical foundation upon which iterative strategies, explicit approximations, and convergence analyses are systematically constructed.

Once a physically coherent and dimensionally closed governing equation has been established, the study proceeds to address the computational challenge posed by its implicit nonlinear structure. The second major objective is therefore algorithmic: to construct a solution strategy that resolves the governing relationship efficiently, stably, and with minimal numerical overhead.

To this end, the fixed-point formulation is systematically refined through the introduction of an adaptive, hydraulically informed initial estimate. Rather than relying on a universal constant starting value, the proposed initialization is formulated as a function of the governing dimensionless parameters, thereby positioning the first iterate in close proximity to the true solution over a wide range of relative conductivity and geometric configurations. This targeted initialization strengthens the contractive behavior of the iteration and significantly reduces the number of updates required to reach engineering-level accuracy. The resulting computational scheme achieves rapid and predictable convergence while maintaining low implementation complexity, making it particularly

well suited for repetitive design calculations, parametric studies, and integration into hydraulic analysis software.

The third objective is to extend the methodology beyond purely iterative schemes by developing explicit, non-iterative approximations that retain high accuracy and controlled error behavior. Whereas the second objective addresses efficient convergence of the implicit governing equation, this third objective focuses on eliminating iteration altogether when a deterministic, closed-form solution is preferred. In engineering practice, explicit formulations offer distinct advantages: they remove the need for convergence criteria, avoid looping procedures, eliminate dependence on stopping tolerances, and ensure transparent, reproducible computation in manual checks, spreadsheet environments, and embedded software routines.

Accordingly, the study derives one-shot analytical approximations constructed directly from the structure of the implicit dimensionless governing equation. These approximations either reduce the nonlinear operator through controlled analytical simplification or incorporate closed-form accelerations of the fixed-point mapping while preserving consistency with the Darcy-Weisbach-RMM framework. Their accuracy is rigorously evaluated over broad practical domains of relative conductivity and sidewall inclination, confirming that rapid computation can be achieved without compromising physical coherence or engineering reliability.

Finally, the study seeks to assess accuracy from a physically meaningful perspective by examining how deviations in the reduced dimensionless variable propagate through the governing transformations to affect the actual relative normal flow depth. This distinction is essential because engineering design and hydraulic analysis ultimately depend on the computed flow depth itself, rather than on intermediate auxiliary parameters introduced for mathematical convenience.

To address this issue, the analysis adopts an amplification-factor viewpoint that quantifies the sensitivity of the physical flow depth to perturbations in the reduced variable. Through this lens, it becomes possible to identify hydraulic regimes in which the nonlinear transformation attenuates numerical deviations, thereby enhancing robustness, and regimes in which it amplifies them, increasing sensitivity. This interpretation establishes a direct connection between numerical error and hydraulic responsiveness of the channel geometry, enabling a rational selection of solution strategies and clarifying when explicit approximations are sufficiently reliable and when iterative refinement remains advisable.

Definition and formulation of the governing problem

The determination of normal depth remains a central issue in the hydraulic design and analysis of open channels. In trapezoidal channels, where the geometry is defined by a bottom width b and side slope m, i.e., m horizontal to 1 vertical (Fig. 1), normal depth y_n governs not only conveyance capacity but also the behavior of gradually varied flow.

The flow is governed by measurable quantities such as the discharge Q, geometric parameters b and m, channel slope S_0, and fluid kinematic viscosity v, together with the

absolute roughness ε, which quantifies the characteristic height of surface irregularities on the channel boundary, including the bed and the side walls of the channel, and influences the frictional resistance encountered by the flow.

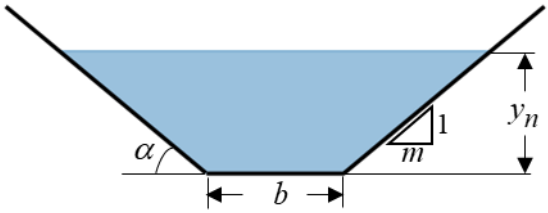

Figure 1: Definition sketch of normal flow depth in a trapezoidal open channel

Traditionally, the computation of normal depth has relied on classical resistance equations, namely the Darcy-Weisbach, Chezy, and Manning formulations. However, each introduces significant limitations. The Darcy-Weisbach equation requires evaluation of the Colebrook-White friction factor, which is implicit and demands repeated trials or graphical interpretation. The Chezy and Manning equations, frequently preferred for their apparent simplicity, are based on resistance coefficients C and n that are routinely treated as constants in practical calculations. Yet this assumption is fundamentally incorrect. As highlighted in the literature (Achour and Amara, 2020a; 2020b), these resistance coefficients depend not only on roughness and viscosity but also directly on the unknown normal depth itself, making it physically unjustifiable to prescribe their values in advance.

Consequently, the formulation of the problem reduces to determining y_n solely from parameters that can be measured with confidence in practice: the discharge, channel geometry, slope, fluid viscosity, and surface roughness. The Rough Model Method (RMM) provides an appropriate path toward this objective. Its principal advantage lies in eliminating the need for uncertain resistance coefficients, whether Chezy, Manning, or Darcy-Weisbach, by introducing a hydraulically equivalent rough model whose parameters circumvent the inconsistencies inherent in conventional methods. In doing so, the RMM establishes a coherent framework for computing normal depth based strictly on physically measurable inputs, as the remainder of the study demonstrates.

RMM basic equations

The present analysis is founded on classical hydraulic relationships, namely the Darcy-Weisbach equation (Darcy, 1854), the Colebrook-White formulation (Colebrook, 1939), and the Reynolds number expression. Herein, the energy slope S_f, where the subscript "f" denotes friction, is considered equal to the geometric slope S_0 of the channel bottom. This equivalence is a direct consequence of uniform-flow theory, in which the gravitational component driving the flow is fully balanced by frictional resistance along the wetted boundary. Therefore, throughout the derivation, the term *energy slope* may be replaced by the channel slope S_0 without loss of generality. Thus, the geometric slope S_0 of an open channel or conduit is governed by the following firmly established Darcy-Weisbach formula (Darcy, 1854). Although this relationship was originally derived for pressurized

circular conduits, Sinniger and Hager (1989) assert that it can also be applied to open channels, irrespective of their geometric configuration.

$$S_0 = \frac{f}{D_h} \frac{Q^2}{2\,g\,A^2} \tag{1}$$

where Q denotes the discharge, g the gravitational acceleration, A the wetted flow area, D_h the hydraulic diameter, and f the friction factor. The latter is evaluated using the well-known Colebrook-White relationship (Colebrook, 1939) as follows:

$$f = -2 \log_{10} \left(\frac{\varepsilon / D_h}{3.7} + \frac{2.51}{R_\mathrm{e} \sqrt{f}} \right) \tag{2}$$

in which ε represents the absolute roughness and Re the Reynolds number. The Reynolds number is in turn expressed as follows:

$$R_\mathrm{e} = \frac{4Q}{P\nu} \tag{3}$$

where v is the kinematic viscosity and P the wetted perimeter.

These three fundamental equations form the basis for the development of the rough model method (RMM) and the subsequent derivation of the non-dimensional implicit relationship used to compute the normal depth.

Geometric and hydraulic characteristics of the rough reference model

In the RMM, all geometric and hydraulic properties of the rough reference model are identified by a subscript "R" that simply denotes "Rough". The model is defined by prescribing an arbitrarily chosen relative roughness of

$$\frac{\varepsilon_\mathrm{R}}{D_{h,\mathrm{R}}} = 0.037 \tag{4}$$

This relatively large relative roughness ensures that the flow regime within the rough model is really "fully rough". Under such conditions, and according to the Colebrook-White formulation, the friction factor attains the following constant value

$$f_\mathrm{R} = \frac{1}{16} \tag{5}$$

corresponding to the Reynolds number $R_\mathrm{e} = R_{\mathrm{e,R}} \to \infty$.

The rough reference model is further characterized by the following characteristics:

(1) the base width b_R such as $b = b_R$

(2) a side slope defined by *m* horizontal to 1 vertical, which corresponds to the geometry of the channel under consideration

(3) a longitudinal slope $S_{0,R} = S_0$

(4) $Q_R = Q$, implying the following

(5) $y_{n,R} \neq y_n$, and even

(6) $y_{n,R} > y_n$

(7) The aspect ratio, also known as the dimensionless normal flow depth is thus:

$$\eta_R = \frac{y_{n,R}}{b} \neq \eta = \frac{y_n}{b}$$

(8) $D_{h,R} = \frac{4A_R}{P_R}$

(9) The wetted perimeter is as follows:

$$P_R = b\left(1 + 2\eta_R\sqrt{1+m^2}\right)$$

(10) The wetted flow area is expressed as follows:

$$A_R = b^2\eta_R\left(1 + m\eta_R\right)$$

(11) The Reynolds number:

$$R_R = \frac{4Q}{P_R\nu}$$

RMM normal flow depth governing relationship

Applying Eq. (1) to the rough reference model yields the following:

$$S_0 = \frac{f_R}{D_{h,R}}\frac{Q^2}{2gA_R^2} \tag{6}$$

Considering the overmentioned characteristics of the rough reference model, and rearranging, Eq. (6) reduces to what follows:

$$\frac{1+2\eta_R\sqrt{1+m^2}}{\eta_R^3\left(1+m\eta_R\right)^3}\left(\frac{Q}{8\sqrt{2gS_0b^5}}\right)^2=1 \tag{7}$$

Eq. (7) can be rewritten in the following form:

$$\frac{1+2\eta_R\sqrt{1+m^2}}{m^3\eta_R^3\left(1+m\eta_R\right)^3}\left(\frac{m^{3/2}Q}{8\sqrt{2gS_0b^5}}\right)^2=1 \tag{8}$$

Let's assume the following relative conductivity relationship:

$$Q^*=\frac{m^{3/2}Q}{8\sqrt{2gS_0b^5}} \tag{9}$$

Substituting Eq. (9) into Eq. (8), the following reduced relationship is obtained:

$$\frac{\left(1+2\eta_R\sqrt{1+m^2}\right)^{1/2}}{\left[m\eta_R\left(1+m\eta_R\right)\right]^{3/2}}Q^*=1 \tag{10}$$

Furthermore, the following change of variables is introduced:

$$z=\left(\frac{1}{2}+m\eta_R\right)^2 \tag{11}$$

Substituting Eq. (11) into Eq. (10), and rearranging, results in the following final relationship:

$$z=\frac{1}{4}+\left(Q^*\right)^{2/3}\left[1+\left(2\sqrt{z}-1\right)\sqrt{1+m^{-2}}\right]^{1/3} \tag{12}$$

This implicit equation can be treated with the Lagrange-Bürmann (Lagrange inversion) theorem, and the resulting series does converge, but only for Q^* small enough, i.e., in a neighborhood of $Q^* = 0$; it is not a globally convergent expansion for arbitrary Q^*. It is suitable, in particular, for low to moderate relative conductivity. For larger Q^*, one should not expect this expansion to remain accurate; in that regime, it is preferable to use direct numerical iteration, as Achour (2014) has already done with the fixed-point method. Moreover, Aitken's Δ^2 acceleration, despite its reputation for improving convergence, still requires approximately 10 to 11 iterative steps before reaching an admissible value of z, demonstrating its comparatively slow performance for this problem.

Although Newton's method is widely regarded as a powerful root-finding strategy, its use for the present implicit governing equation is neither convenient nor computationally efficient. The primary limitation stems from the fact that Newton's method requires not only the evaluation of the residual at every iteration but also the repeated computation of the derivative of a function whose structure is highly nonlinear. In this case, the derivative contains nested square-root terms and fractional powers, and its expression is lengthy and cumbersome. As a result, each Newton iteration becomes significantly more expensive than a simple algebraic update. Furthermore, the accuracy and stability of Newton's method depend critically on the correctness and numerical reliability of the derivative. Any slight loss of precision in computing this derivative directly affects the Newton step, potentially slowing convergence or causing overshooting when the initial guess is not extremely close to the true root. This sensitivity imposes an additional burden, as it demands high numerical precision and careful implementation, conditions that reduce the practical attractiveness of the method. For these reasons, its derivative burden, higher computational cost, sensitivity to the initial guess, and lack of guaranteed convergence across all conditions, Newton's method is not an appropriate or efficient numerical tool for solving the implicit governing Eq. (12).
Another drawback is that Newton's method does not guarantee convergence for all initial guesses. Given the nonlinear form of the governing equation, the user must ensure that the starting value lies within the basin of attraction of the root. This requirement diminishes the robustness of the method and can lead to divergence or oscillation if the initial guess is not chosen judiciously. In engineering practice, where a method must be reliable across a wide range of hydraulic and geometric conditions, such sensitivity is undesirable.

Because the governing implicit Eq. (12) contains nested nonlinearities involving both square-root and cube-root terms, no analytical manipulation can isolate the unknown z in closed form. General inversion techniques or series-based methods are either inapplicable or produce divergent expansions, confirming the impossibility of deriving an exact analytical expression.

In contrast, the fixed-point method avoids all derivative calculations and relies solely on direct algebraic substitution. Despite its simplicity, it demonstrates strong and remarkably stable convergence over the entire domain considered. The method consistently yields accurate values of z within only a handful of iterations, even when the geometry becomes steep or the hydraulic nonlinearity increases. Because each iteration involves only elementary operations and no derivative evaluation, the fixed-point method is computationally lightweight, easy to implement, and far more suitable for routine hydraulic computation. As such, it constitutes the most accurate and operationally efficient method for solving Eq. (12).

Eq. (12) is the implicit RMM governing equation for z. From a mathematical standpoint, this equation is best classified as an implicit nonlinear algebraic fixed-point equation. In earlier work (Achour, 2014), Eq. (12) was solved using a fixed-point iteration, which required six to seven steps to reach an acceptable final value of z. This is essentially due to the choice of the guess value $z_0 = 1/4$, derived from Eq. (11) for $\eta_R = 0$.

However, in the present study, the initial guess z_0 is not treated as a constant; rather, it is computed as an improved function of both the relative conductivity Q^* and the side slope m as follows:

$$z_0 = \frac{1}{4} + \left(2\sqrt{1 + m^{-2}}\right)^{2/5} \left(Q^*\right)^{4/5} \tag{13}$$

Eq. (13) was derived from an in-depth limited development study. This improvement translates into reduced computational effort, since it allows reaching acceptable final z value after only one or two iterative steps.

While the constant guess z_0 =1/4 remains attractive for its simplicity and universality, the adaptive guess derived from Eq. (13) provides a more refined and hydraulically meaningful starting point. Its incorporation into improved iterative schemes enhances numerical stability, accelerates convergence, and strengthens the overall efficiency of the computational process.

As it can be seen later, for $10 \le \alpha\,(^\circ) \le 80$ and $0.1 \le Q^* \le 4$, where α is the inclination angle of the trapezoidal channel sides with respect to horizontal (Fig. 1), Eq. (12), based on Eq. (13), produces a maximum deviation of about 0.007 %. The worst case occurs at $\alpha = 80°$ with deviations of about 0.007004 %.

The values of z are derived from Eq. (12), while adopting the following iterative process:

$$z_1 = \frac{1}{4} + \left(Q^*\right)^{2/3} \left[1 + \left(2\sqrt{z_0} - 1\right)\sqrt{1 + m^{-2}}\right]^{1/3} \tag{12a}$$

$$z_2 = \frac{1}{4} + \left(Q^*\right)^{2/3} \left[1 + \left(2\sqrt{z_1} - 1\right)\sqrt{1 + m^{-2}}\right]^{1/3} \tag{12b}$$

$$z_3 = \frac{1}{4} + \left(Q^*\right)^{2/3} \left[1 + \left(2\sqrt{z_2} - 1\right)\sqrt{1 + m^{-2}}\right]^{1/3} \text{ …and so on.} \tag{12c}$$

The iterative process stops when z_k and z_{k+1} are sufficiently close.

Once z is determined, the sought relative normal flow depth, in the rough reference model, is recovered from Eq. (11) as follows:

$$\eta_R = \left(\sqrt{z} - \frac{1}{2}\right) m^{-1} \tag{11a}$$

The rough model method states that any linear dimension "L" of a conduit or channel and the linear dimension "L_R" of its rough reference model are related by the following relationship, applicable to the entire domain of the turbulent flow:

$$L = \psi L_R \tag{14}$$

The parameter ψ is defined as the dimensionless correction factor of linear dimension, less than unity, which is governed by the following relationship (Achour and Bedjaoui, 2006; Achour and Bedjaoui, 2012):

$$\psi = 1.35\left[-\log\left(\frac{\varepsilon / D_{h,\mathrm{R}}}{4.75} + \frac{8.5}{R_{\mathrm{e,R}}}\right)\right]^{-2/5} \tag{15}$$

All parameters in Eq. (15) are known, which allows explicitly calculating ψ.

Computation steps of the normal flow depth

To determine the normal depth y_n, the following parameters must be specified: Q, b, S_0, m, ε, and ν. It should be emphasized, first, that all of these quantities are directly measurable in practice, and second, that no flow-resistance coefficient, such as the Chézy coefficient or Manning's roughness coefficient, is required.
The recommended procedure for computing the normal depth y_n is as follows:

1) Compute the relative conductivity Q* using Eq. (9).
2) Calculate the value of z using Eq. (12) while adopting the described iterative process,
3) considering the guess z_0 value derived from Eq. (13).
4) With the calculated final value of z, compute the aspect ratio η_R in the rough reference model using Eq. (11a).
5) Consequently, this allows deriving the following rough reference model parameters: the wetted perimeter P_R, the water wetted area A_R, hence the hydraulic diameter $D_{h,R}$, and Reynolds number R_R.
6) Thus, compute the non-dimensional correction factor of linear dimension ψ by the use of Eq. (15).
7) Assign to the rough reference model the new linear dimension $b_R = b/\psi$, in accordance with Eq. (14), and derive the corresponding value of the relative conductivity Q* using Eq. (9).
8) With the new calculated value of Q*, compute z according to the step (2). Stop the iteration process at the step z_4.
9) By introducing this value of z in Eq. (11a), we obtain the aspect ratio η_R in the rough reference model equal to the sought aspect ratio $\eta = y_n/b$; Thus, the required normal depth y_n is then worked out.

Table 1 presents a detailed numerical evaluation of the fixed-point iterative process used to compute the quantities z_3 and z_4 for a trapezoidal channel with an inclination angle α = 45°. The relative conductivity Q^* spans the wide interval $0.10 \leq Q^* \leq 4$, which allows assessment of the method across both low-conductivity and high-conductivity flow regimes. The last column reports the relative deviation (%) between the two iterations,

offering a direct measure of the contraction properties and stability of the fixed-point approach.

Across the entire range of Q^*, the deviations remain extremely small, consistently sub-0.007 %. The worst case occurs at the end-point $Q^* = 3.2$. Such low discrepancies demonstrate that the fixed-point mapping behaves strongly contractively under the chosen conditions, especially the choice of the guess z_0 expressed by Eq. (13). The proximity of z_3 and z_4 confirms that the iteration stabilizes rapidly and that only a small number of iterations is required to achieve acceptable accuracy.

For low values of Q^*, the deviations are exceptionally small, typically less than 0.001 %. This reflects: (1) a smoother response of the governing hydraulic equations in the low-flow regime, (2) weak nonlinearities in the computation of z, and (3) a highly stable fixed-point function.

As Table 1 reveals, when the relative conductivity increases and the deviation between successive iterations decreases, this indicates that the fixed-point method is entering a regime where the governing relationship becomes progressively more stable and less sensitive to small numerical perturbations. In practical terms, larger values of the relative conductivity correspond to deeper and more energetic flow conditions in the rough reference model. Under these conditions, the hydraulic response becomes smoother: incremental changes in flow depth produce smaller proportional variations in the geometric and hydraulic properties of the section. As a result, the iterative function being evaluated changes very little from one step to the next, and the numerical solution converges more rapidly. From a numerical standpoint, this behavior means that the mapping used in the fixed-point procedure becomes more strongly contractive as the relative conductivity increases. The "pull" of the iteration toward its true solution strengthens, and the discrepancy between two consecutive iterates diminishes steadily. The fact that deviations fall from about 0.002% at low relative conductivity to values as small as 0.007% in the upper range shows that the iteration is operating in its most favorable zone at high discharge levels. Hydraulically, the outcome reflects the stabilising influence of deeper flows: as the flow becomes larger, the influence of local geometric irregularities and nonlinearities decreases in relative importance, and the overall behavior becomes more regular. Thus, the reduction in deviation with increasing relative conductivity is not only expected but is also a sign of excellent numerical robustness. It confirms that the iterative procedure performs best under high-flow conditions and that the solution obtained in this range is extremely reliable.

The deviation column in Table 1 displays a smooth, nearly linear progression from the lowest to the highest values of Q^*. This smoothness indicates: numerical regularity, absence of oscillatory behavior, and no evidence of divergence or iteration instability.
Such behavior is desirable for engineering applications, as it confirms that the method remains predictable and well-conditioned over a broad hydraulic domain.

With regard to practical implications: The fixed-point approach is both efficient and reliable for computing z at $\alpha = 45°$. The deviations remain under control even at high relative conductivity, ensuring accurate estimation of normal-flow depth-related

parameters. The method is particularly robust at low and intermediate Q^*, where convergence is strongest. The progressive increase in deviation at high Q^* is consistent with enhanced geometric and hydraulic nonlinearities, yet never threatens the convergence of the method.

In short, Table 1 clearly demonstrates that the fixed-point method performs exceptionally well under the tested conditions. The deviations between successive iterates remain extremely small, even as the hydraulic nonlinearity intensifies with increasing Q^*. This confirms that the iterative scheme is numerically stable, rapidly convergent, and suitable for accurate hydraulic computations over an extensive range of relative conductivity.

Table 1: Results of the iterative computation of z_3 and z_4 using the fixed-point method for a trapezoidal channel with $\alpha = 45°$ over the range $0.10 \leq Q^* \leq 4$

Q^*	$(Q^*)^{2/3}$	α (°), $m = 1$	z_3	z_4	Deviation (%)
0.1	0.21544347	45	0.50136836	0.50138017	0.00235489
0.2	0.34199519	45	0.67417703	0.67418784	0.00160348
0.3	0.44814047	45	0.82944778	0.82944993	0.00025938
0.4	0.54288352	45	0.97464234	0.9746329	0.00096881
0.5	0.62996052	45	1.11286808	1.11284602	0.00198206
0.6	0.71137866	45	1.24581581	1.24578094	0.0027994
0.7	0.78837352	45	1.37454239	1.37449486	0.00345781
0.8	0.86177388	45	1.49976791	1.49970806	0.00399094
0.9	0.93216975	45	1.62201284	1.62194106	0.00442565
1.0	1	45	1.74166998	1.74158668	0.00478264
1.1	1.06560224	45	1.85904566	1.85895126	0.00507775
1.2	1.12924323	45	1.97438506	1.97427996	0.00532311
1.3	1.19113843	45	2.08788859	2.08777317	0.0055281
1.4	1.25146495	45	2.19972294	2.19959755	0.00570006
1.5	1.3103707	45	2.31002873	2.30989372	0.00584476
1.6	1.36798076	45	2.41892616	2.41878183	0.0059668
1.7	1.42440213	45	2.52651899	2.52636564	0.00606985
1.8	1.47972724	45	2.63289771	2.6327356	0.0061569
1.9	1.53403664	45	2.73814181	2.73797121	0.0062304
2.0	1.58740105	45	2.84232169	2.84214284	0.00629234
2.1	1.639883	45	2.94550008	2.94531321	0.00634439
2.2	1.69153811	45	3.0477332	3.04753852	0.00638794
2.3	1.74241616	45	3.14907171	3.14886941	0.00642413
2.4	1.7925619	45	3.24956146	3.24935174	0.00645396
2.5	1.84201575	45	3.34924416	3.34902719	0.00647825
2.6	1.89081439	45	3.44815789	3.44793384	0.00649771
2.7	1.93899122	45	3.54633751	3.54610654	0.00651295
2.8	1.98657678	45	3.64381512	3.64357738	0.00652448
2.9	2.03359906	45	3.74062028	3.74037592	0.00653275

3.0	2.08008382	45	3.83678037	3.83652951	0.00653816
3.1	2.12605484	45	3.93232074	3.93206353	0.00654103
3.2	2.17153409	45	4.02726501	4.02700156	0.00654167
3.3	2.21654197	45	4.12163515	4.12136558	0.00654033
3.4	2.26109744	45	4.21545171	4.21517614	0.00653723
3.5	2.30521815	45	4.30873392	4.30845245	0.00653259
3.6	2.34892058	45	4.4014998	4.40121253	0.00652656
3.7	2.39222018	45	4.49376629	4.49347332	0.00651931
3.8	2.43513138	45	4.58554933	4.58525077	0.00651096
3.9	2.47766777	45	4.67686396	4.67655989	0.00650166
4.0	2.5198421	45	4.76772437	4.76741487	0.00649149
					Max. ≈ 0.0065416 %

Table 2 presents the maximum deviations between the third and the fourth fixed-point iterates over the full hydraulic range $0.1 \leq Q^* \leq 4$, for inclination angles α spanning from 10° to 80°.

Table 2: Maximum deviations (%) between z_3 and z_4 produced by the RMM governing Eq. (12), using the fixed-point method within $0 \leq Q^* \leq 4$ and $10° \leq \alpha \leq 80°$

α (°)	Maximum deviation between z_3 and z_4 (%)
10	0.007102992
15	0.00676709
20	0.006305347
25	0.005679109
30	0.004974859
35	0.004132599
40	0.00411607
45	0.006541669
50	0.009826568
55	0.014323208
60	0.020499241
65	0.029125056
70	0.041504933
75	0.060225968
80	0.090365472

The deviations, reported in Table 2, provide a direct measure of the contractive strength and numerical stability of the fixed-point mapping used to solve the governing implicit

Eq. (12). The values reported reveal several important patterns regarding both the behavior of the iterative scheme and the hydraulic characteristics of trapezoidal channel geometry. For α between 10° and 50°, the deviations remain extremely small, varying between 0.007% and 0.0098 %. This indicates that the fixed-point iteration operates within a very favorable region of the governing relationship, where the flow geometry evolves smoothly with flow depth and the nonlinearity of the hydraulic response is relatively weak. Under these conditions, the iteration is strongly contractive, and convergence to the solution is achieved rapidly and reliably.

Between 10° and 40°, the deviations decrease steadily, reaching their minimum value of approximately 0.004 % at $\alpha = 40°$. This interval corresponds to a geometric configuration in which the balance between cross-sectional area and wetted perimeter changes in a particularly regular manner. The governing equation becomes locally smoother, and the fixed-point mapping exhibits its strongest convergence behavior. This region represents the optimal convergence zone for the method.

When the inclination angle exceeds 40°, the deviations begin to rise, reaching: ~ 0.03% at 65°, ~ 0.04% at 70°, ~ 0.06% at 75°, and ~ 0.09% at 80°. This upward trend reflects the increasing hydraulic nonlinearity associated with steep and near-vertical channel walls. As the geometry becomes more sensitive to small changes in flow depth, the iterative mapping loses part of its contractive strength, leading to slightly larger, but still very small, differences between successive iterates.

Despite the increase at high angles, the maximum deviation remains exceptionally low even at $\alpha = 80°$. A deviation of only 0.09% confirms that the fixed-point method remains stable, reliable, and far from any numerical instability or divergence. The smoothness of the trend and the absence of oscillatory or irregular behavior further attest to the robustness of the approach.

All deviations reported in Table 2 are far below the uncertainty typically associated with hydraulic parameters such as channel roughness, energy slope, and geometric measurements. In practical engineering terms, convergence at the level of better than one-tenth of one percent across all wall inclinations represents excellent numerical performance. This means the method provides highly accurate results regardless of whether the trapezoidal channel is shallow-sided or nearly vertical.

In short, Table 2 clearly demonstrates that the fixed-point method exhibits strong, consistent, and reliable convergence over the entire range of inclination angles. Deviations remain exceptionally low for all geometries, with optimal performance around intermediate inclinations and modest increases for the steepest walls, yet never approaching levels that threaten numerical stability. These results confirm that the method is robust, efficient, and well-suited for computing the normal depth in trapezoidal channels across a wide variety of hydraulic and geometric conditions.

Based on the values reported in Table 2, Fig. 2 depicts the maximum relative deviation between the third and the fourth fixed-point iterates, denoted z_3 and z_4, evaluated over the

following full range of the relative discharge conductivity $0.1 \leq Q^* \leq 4$, as a function of the sidewall inclination angle α of the trapezoidal channel. The curve provides important insight into how channel geometry influences the numerical behavior of the fixed-point scheme used to solve the governing implicit Eq. (12).

Because the difference $|z_4 - z_3|$ represents the residual after three fixed-point updates, this deviation provides a direct measure of the convergence rate and numerical stability of the iterative scheme applied to the implicit governing equation.

Fig. 2 reveals a systematic and physically meaningful dependence of the convergence behavior on the inclination angle:

(1) For moderate wall inclinations, roughly $10° \leq \alpha \leq 48°$, the maximum deviation remains extremely small, typically below 0.01 %, and exhibits a shallow minimum around $\alpha \approx 40°$. In this range, the difference between the third and fourth iterates is practically negligible, indicating that the fixed-point process has essentially converged after only three iterations for all values of $Q*$ considered; and (2) as α increases beyond approximately 55°, the deviation grows progressively and becomes more pronounced for steep sidewalls. Near $\alpha = 80°$, the deviation reaches 0.09 %, reflecting a reduced contraction rate of the fixed-point mapping in this geometric regime. This behavior is fully consistent with the structure of the governing equation, as larger inclination angles amplify the nonlinear contribution of the following parameter:

$$\sqrt{1 + m^{-2}}$$

thereby slowing the convergence of successive iterates.

Fig. 2 clearly demonstrates the following: (1) Three fixed-point iterations are sufficient to achieve acceptable accuracy for practical purposes when $\alpha \leq 50°$, across the entire $Q*$ domain investigated; (2) Even for very steep sidewalls, the residual after three iterations remains below 0.1 %, confirming the robustness and unconditional stability of the fixed-point scheme; and (3) The increase in deviation at high α does not indicate divergence, but rather a slower asymptotic convergence, which could be remedied, if necessary, by performing one additional iteration.

From an engineering and computational perspective, Fig. 2 supports the following conclusions: (1) The fixed-point formulation used to solve the implicit normal-flow depth equation is highly efficient, requiring only a small number of iterations for convergence; (2) For the vast majority of trapezoidal channel geometries encountered in practice ($\alpha \leq$ 55°, three iterations are sufficient, making the method both fast and reliable; and (3) For extremely steep walls, the method remains fully applicable, with the option of a fourth iteration ensuring very high accuracy when required.

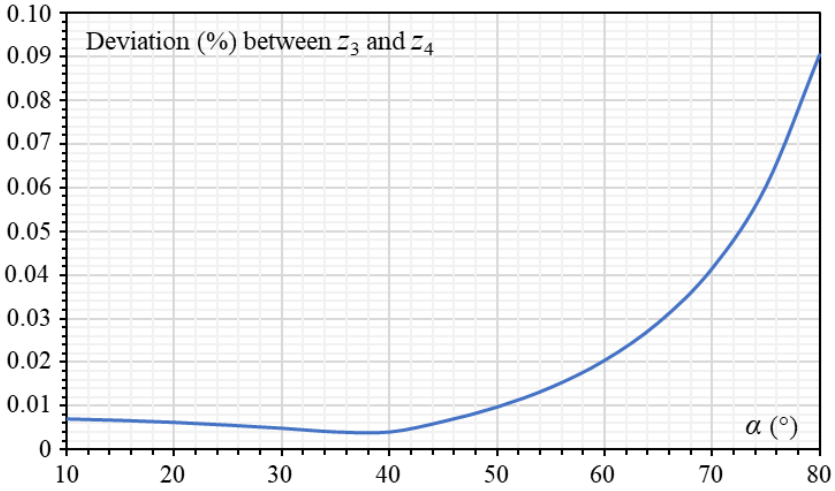

Figure 2: Distribution of the maximum deviation between z_3 and z_4 with respect to the inclination angle α (°), using the fixed-point method, within the full range $0.1 \leq Q^* \leq 4$

Numerical example

The following data were collected on a trapezoidal open channel:

The discharge $Q = 0.12528368$ m^3/s, the inclination angle of the side walls with respect to the horizontal $\alpha = 45°$ ($m = 1$), a base width $b = 0.5$ m, the bed slope $S_0 = 0.0001$, the kinetic viscosity of the flowing liquid $v = 10^{-6}$ m^2/s, and the absolute roughness $\varepsilon = 0.001$ m. Determine the normal flow depth.

1. The previous data allow calculating the relative conductivity as follows, according to Eq. (9):

$$Q^* = \frac{m^{3/2} Q}{8\sqrt{2g S_0 b^5}}$$

Thus

$$Q^* = \frac{1^{3/2} \times 0.12528368}{8 \times \sqrt{2 \times 9.81 \times 0.0001 \times 0.5^5}} = 2$$

2. The initial guess, according to Eq. (13), is as follows:

$$z_0 = \frac{1}{4} + \left(2\sqrt{1 + m^{-2}}\right)^{2/5} \left(Q^*\right)^{4/5}$$

which gives the following final result:

$$z_0 = 2.88901582$$

3. With z_0, the iterative process carried out on the implicit equation (12), as described previously, allowed us to deduce the following result:

$z_3 = 2.84232169$

4. The aspect ratio in the rough reference model is given by Eq. (11a) as follows:

$$\eta_{\mathrm{R}} = \left(\sqrt{z_3} - \frac{1}{2}\right) m^{-1}$$

Thus

$$\eta_{\mathrm{R}} = \left(\sqrt{2.84232169} - \frac{1}{2}\right) \times 1 = 1.18591865$$

5. This result allows deriving the following hydraulic parameters:

5.1. The wetted perimeter in the rough reference model:

$$P_{\mathrm{R}} = b\left(1 + 2\eta_{\mathrm{R}}\sqrt{1 + m^2}\right)$$

So

$$P_{\mathrm{R}} = 0.5 \times \left(1 + 2 \times 1.18591865 \times \sqrt{1+1}\right) = 2.177142237\,\mathrm{m}$$

5.2. The wetted area in the rough reference model is given as follows:

$$A_{\mathrm{R}} = b^2 \eta_{\mathrm{R}} \left(1 + m\eta_{\mathrm{R}}\right)$$

Thus

$$A_{\mathrm{R}} = 0.5^2 \times 1.18591865 \times \left(1 + 1 \times 1.18591865\right) = 0.64808042\,\mathrm{m}^2$$

5.3. The hydraulic diameter in the rough reference model is given as follows:

$$D_{h,\mathrm{R}} = \frac{4A_{\mathrm{R}}}{P_{\mathrm{R}}}$$

So

$$D_{h,\mathrm{R}} = \frac{4 \times 0.64808042}{2.177142237} = 1.19069928\,\mathrm{m}$$

6. Thus, the Reynolds number characterizing the flow in the rough reference model is as follows:

$$R_{\mathrm{R}} = \frac{4Q}{P_{\mathrm{R}}\,\nu}$$

Thus

$$R_{\mathrm{R}} = \frac{4\times 0.12528368}{2.17714224\times 10^{-6}} = 230180.055$$

7. The previous results allow computing the non-dimensional correction factor of linear dimension ψ by the use of Eq. (15), as follows:

$$\psi = 1.35\left[-\log\left(\frac{\varepsilon / D_{h,\mathrm{R}}}{4.75} + \frac{8.5}{R_{\mathrm{e,R}}}\right)\right]^{-2/5}$$

That is

$$\psi = 1.35\times\left[-\log\left(\frac{0.001/1.19069928}{4.75} + \frac{8.5}{230180.055}\right)\right]^{-2/5} = 0.802530615$$

8. Now, assign to the rough reference model the following new base width in accordance with the fundamental RMM Eq. (14):

$$b_{\mathrm{R}} = \frac{b}{\psi}$$

So

$$b_{\mathrm{R}} = \frac{0.5}{0.802530615} = 0.623029191\,\mathrm{m}$$

9. The corresponding value of the new relative conductivity is as follows:

$$Q^{*} = \frac{m^{3/2}Q}{8\sqrt{2g\,S_0\,b^5}}$$

That is

$$Q^{*} = \frac{1^{3/2}\times 0.12528368}{8\times\sqrt{2\times 9.81\times 0.0001\times 0.62302919^5}} = 1.15394212$$

10. The new initial guess is as follows:

$$z_0 = \frac{1}{4} + \left(2\sqrt{1 + m^{-2}}\right)^{2/5} \left(Q^*\right)^{4/5}$$

The final result is the following:

$$z_0 = 1.94967238$$

11. Using this new guess value, the iterative process applied on the implicit Eq. (12), allowed deriving the following result: $z_3 = 1.92150146$

12. Thus, Eq. (11a) gives the sought aspect ratio in the considered channel as follows:

$$\eta_{\mathrm{R}} = \eta = \left(\sqrt{z_3} - \frac{1}{2}\right) m^{-1}$$

Thus

$$\eta = \left(\sqrt{1.92150146} - \frac{1}{2}\right) \times 1 = 0.88618233$$

13. Thus, the required normal flow depth is as follows:

$$y_n = b\eta$$

So

$$y_n = 0.5 \times 0.88618233 = 0.44309117\,\mathrm{m}$$

14. This ultimate step aims to verify the validity of the calculations by determining the discharge Q using Chezy's equation. The discharge so calculated should be equal to the discharge given in the problem statement. Chezy's equation expresses the discharge Q as follows:

$$Q = C\,A\sqrt{R_h S_0}$$

where C is the Chezy's coefficient, and R_h is the hydraulic radius.

According to the rough model method (RMM), the coefficient C is related to ψ by the following formula:

$$C = \frac{8\sqrt{2g}}{\psi^{5/2}}$$

Hence

$$C = \frac{8 \times \sqrt{2 \times 9.81}}{0.80253062^{5/2}} = 61.4165569 \text{ m}^{0.5} / s$$

The wetted perimeter in the trapezoidal channel is as follows:

$$P = b\left(1 + 2\eta\sqrt{1 + m^2}\right)$$

So

$$P = 0.5 \times \left(1 + 2 \times 0.88618233 \times \sqrt{1+1}\right) = 1.75325107 \text{ m}$$

The water area is given as follows:

$$A = b^2\eta\left(1 + m\eta\right)$$

That is

$$A = 0.5^2 \times 0.88618233 \times \left(1 + 1 \times 0.88618233\right) = 0.41787537 \text{ m}^2$$

The hydraulic radius is then:

$$R_h = \frac{A}{P} = \frac{0.41787537}{1.75325107} = 0.23834314 \text{ m}$$

Furthermore, the discharge Q according to Chezy's equation is as follows:

$$Q = C\,A\sqrt{R_h S_0} = 61.4165569 \times 0.41787537 \times \sqrt{0.23834314 \times 0.0001}$$

Thus

$$Q = 0.12529495 \text{ m}^3 / s$$

The deviation between the calculated discharge and the discharge given in the problem statement is as follows:

$$\frac{\Delta Q}{Q} = 100 \times \frac{\left|0.12529495 - 0.12528368\right|}{0.12528368} = 0.00899559\,\% \approx 0.009\,\%$$

This result clearly indicates that the method and the related relationships are highly reliable.

Achour and Amara explicit accurate analytical approximation

Approximate model presentation

The following proposed one-shot explicit formulation constitutes a rigorous and efficient approximation of the implicit normal-flow depth relationship governing flow in trapezoidal channels. It is constructed on a physically consistent reference state that captures the dominant behavior of the solution over the entire range of practical relative conductivity, while remaining exact in the limiting case of vanishing flow. Rather than relying on iterative convergence, the method replaces the nonlinear structure of the governing relationship with a locally controlled representation that preserves its intrinsic hydraulic meaning.

The core strength of the approach lies in the way the nonlinearity associated with the cube-root dependence is treated. By performing a controlled local linearization around a judiciously chosen reference depth, the implicit equation is reduced to a closed, directly solvable expression. This procedure is neither empirical nor heuristic; it relies solely on the analytical properties of the original equation and ensures that higher-order effects remain bounded and predictable.

As a result, the derived expression for z(app), where "app" denotes "approximate", provides a true one-shot solution: the reduced normal flow depth z is obtained directly, without iterations, stopping criteria, or sensitivity to initial guesses. Despite this simplification, the approximation retains a high level of accuracy across all relevant geometries and discharge conditions. The influence of channel sidewall inclination is fully accounted for in an analytical manner, which guarantees uniform performance for mild as well as relatively steep trapezoidal sections.

From both a computational and practical standpoint, the proposed formulation represents a substantial improvement over classical fixed-point scheme. It dramatically reduces computational effort while maintaining consistency with the exact implicit solution. This makes the approximation particularly well suited for design calculations, parametric studies, and implementation in engineering software where robustness, speed, and clarity are essential.

In short, the derived explicit expression successfully reconciles analytical rigor with practical applicability, offering a reliable and efficient alternative to iterative solution methods for the normal-flow depth problem in trapezoidal open channels.

Approximate model formulation

Let's start with writing the implicit governing Eq. (12) in a compact form. To do so, let's define the following:

$$\omega = \left(Q^*\right)^{2/3} \tag{16}$$

and

$$s = \sqrt{1 + m^{-2}} \tag{17}$$

Substituting Eqs. (16) and (17) into Eq. (12) yields the following:

$$z = \frac{1}{4} + \omega\left[1 + s\left(2\sqrt{z} - 1\right)\right]^{1/3} \tag{18}$$

Define the fixed-point map which is exactly Eq. (12) written as follows:

$$z = \Phi\left(z\right) \tag{19}$$

Thus, the following can be written:

$$\Phi\left(z\right) = \frac{1}{4} + \omega\left[1 + s\left(2\sqrt{z} - 1\right)\right]^{1/3} \tag{20}$$

Then, Eq. (12) is explicitly stated as the governing implicit fixed-point equation for z.

For sufficiently large z, the bracket in Eq. (20) becomes dominated by the $\sqrt{z}$ term, so that writing the following:

$$1 + s\left(2\sqrt{z} - 1\right) = 1 - s + 2s\sqrt{z} \approx 2s\sqrt{z} \tag{21}$$

Inserting the previous result into Eq. (18) yields the following:

$$z \approx \frac{1}{4} + \omega\left(2s\sqrt{z}\right)^{1/3} \tag{22}$$

Now, compute the cube root carefully as follows:

$$\left(2s\sqrt{z}\right)^{1/3} = \left(2s\right)^{1/3}\left(\sqrt{z}\right)^{1/3} = \left(2s\right)^{1/3} z^{1/6} \tag{23}$$

Substituting this result into Eq. (22) provides what follows:

$$z \approx \frac{1}{4} + \omega\left(2s\right)^{1/3} z^{1/6} \tag{24}$$

For the dominant balance, i.e., large z, 1/4 can be dropped compared to z, allowing writing Eq. (24) as follows:

$$z \approx \omega\left(2s\right)^{1/3} z^{1/6} \tag{25}$$

In Eq. (25), bring powers of z together such that writing the following:

$$z^{1-1/6} = z^{5/6} \approx \omega\left(2s\right)^{1/3} \tag{26}$$

Raise both sides of Eq. (26) to 6/5; thus, the following can be written:

$$z \approx \left[\omega(2s)^{1/3}\right]^{6/5} = \omega^{6/5}(2s)^{2/5} \tag{27}$$

From Eq. (16), one may write the following:

$$\omega^{6/5} = \left[\left(Q^*\right)^{2/3}\right]^{6/5} = \left(Q^*\right)^{4/5} \tag{28}$$

Therefore, Eq. (27) becomes as follows:

$$z \approx \left(Q^*\right)^{4/5}(2s)^{2/5} \tag{29}$$

To also satisfy the exact limit $Q* = 0 \Rightarrow z = 1/4$, one may choose the following:

$$z_0 = \frac{1}{4} + \left(Q^*\right)^{4/5}(2s)^{2/5} \tag{30}$$

Let's define the following:

$$B(z) = 1 + s\left(2\sqrt{z} - 1\right) \tag{31}$$

Thus, Eq. (20) can be rewritten as follows:

$$\Phi(z) = \frac{1}{4} + \omega\left[B(z)\right]^{1/3} \tag{32}$$

Let's now approximate $\Phi(z)$ to first order about $z = z_0$; thus, the following can be written:

$$\Phi(z) \approx \Phi(z_0) + \Phi'(z_0)(z - z_0) \tag{33}$$

Because the true solution satisfies $z = \Phi(z)$, let's impose the following:

$$z \approx \Phi(z_0) + \Phi'(z_0)(z - z_0) \tag{34}$$

Let's solve this algebraically for z such as writing the following:

$$z - z\,\Phi'(z_0) = \Phi(z_0) - z_0\,\Phi'(z_0) \tag{35}$$

Eq. (35) can be rewritten as follows:

$$z\left[1 - \Phi'(z_0)\right] = \Phi(z_0) - z_0\,\Phi'(z_0) \tag{36}$$

Thus, the following result is obtained:

$$z(\text{app}) = \frac{\Phi\left(z_0\right) - z_0\,\Phi^{'}\left(z_0\right)}{1 - \Phi^{'}\left(z_0\right)} \tag{37}$$

Let's recall that "app" denotes "approximate".

Now compute the derivative $\Phi'(z)$ explicitly. To do so, recall Eq. (32) as follows:

$$\Phi\left(z\right) = \frac{1}{4} + \omega\left[B(z)\right]^{1/3} \tag{32}$$

Thus, the following can be written:

$$\Phi^{'}\left(z\right) = \frac{1}{3}\omega\left[B(z)\right]^{-2/3} B^{'}\left(z\right) \tag{38}$$

Now, expand Eq. (31) as follows:

$$B\left(z\right) = 1 + s\left(2\sqrt{z} - 1\right) = 1 - s + 2s\sqrt{z} \tag{39}$$

On other side, therefore, the following can be written:

$$\frac{d}{dz}\sqrt{z} = \frac{1}{2\sqrt{z}} \tag{40}$$

Thus, from Eq. (39), the following is written:

$$B^{'}\left(z\right) = 2s\,\frac{1}{2\sqrt{z}} = \frac{s}{\sqrt{z}} \tag{41}$$

Substituting this result into Eq. (38) yields what follows:

$$\Phi^{'}\left(z\right) = \frac{1}{3}\omega\left[B(z)\right]^{-2/3}\frac{s}{\sqrt{z}} \tag{42}$$

Now, evaluate at z_0. Let's rewriting Eq. (31) as follows:

$$B_0\left(z\right) = B\left(z_0\right) = 1 + s\left(2\sqrt{z_0} - 1\right) \tag{43}$$

Thus, Eq. (32) becomes as follows:

$$\Phi\left(z_0\right) = \frac{1}{4} + \omega B_0^{1/3} \tag{44}$$

In addition, Eq. (42) is written in the following form:

$$\Phi'\left(z_0\right) = \frac{1}{3}\omega\, B_0^{-2/3}\frac{s}{\sqrt{z_0}} \tag{45}$$

Thus, From Eq. (37), the final one-shot approximation is written as follows:

$$z(\text{app}) = \frac{\left(\frac{1}{4} + \omega B_0^{1/3}\right) - z_0\left(\frac{1}{3}\omega\, B_0^{-2/3}\frac{s}{\sqrt{z_0}}\right)}{1 - \left(\frac{1}{3}\omega\, B_0^{-2/3}\frac{s}{\sqrt{z_0}}\right)} \tag{46}$$

It is useful to recall the following:

$$\omega = \left(Q^*\right)^{2/3} \tag{16}$$

$$s = \sqrt{1 + m^{-2}} \tag{17}$$

$$z_0 = \frac{1}{4} + \left(Q^*\right)^{4/5}\left(2s\right)^{2/5} \tag{30}$$

$$B_0 = 1 + s\left(2\sqrt{z_0} - 1\right) \tag{43}$$

Fig. 3 illustrates the maximum relative deviation in the reduced normal flow depth z(app) given by Eq. (46), expressed in percent, as a function of the sidewall inclination angle α expressed in degree. The deviation is evaluated by comparison with the reference solution obtained from the implicit governing Eq. (12).

From Fig. 3, a clear and physically consistent trend is observed. For moderate inclination angles, approximately $10° \leq \alpha \leq 55°$, the deviation remains extremely small, typically below 0.02 %, and reaches a minimum close to $\alpha \approx 45°$. In this interval, the proposed explicit approximation [Eq. (46)] reproduces the exact implicit solution with very high fidelity, far exceeding the accuracy requirements of most engineering applications.

As the inclination angle increases beyond about 55°, the deviation begins to grow progressively and accelerates for α greater or equal to 65°, reaching values on the order of 0.2 % near $\alpha = 80°$. Although this level of error remains modest in absolute terms, it reflects the increasing nonlinearity of the governing equation as the channel sides become steeper. In this regime, the following term appearing in Eq. (12):

$$\sqrt{1 + m^{-2}}$$

becomes dominant, amplifying the sensitivity of the solution to higher-order effects that are only partially captured by the controlled algebraic approximation.

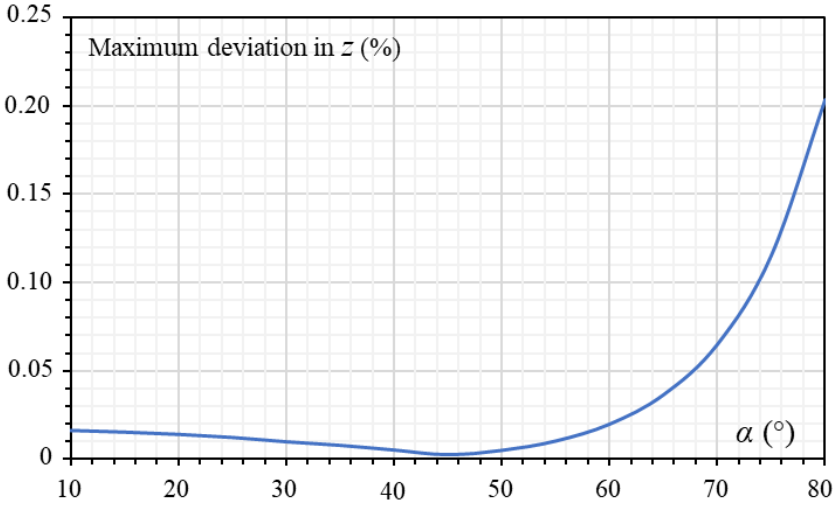

Figure 3: Maximum deviation (%) produced by the approximate Eq. (46) in the computation of *z*, with respect to the inclination angle *α* (°), within the full range $0.1 \leq Q^* \leq 4$

In addition, it is fully justified to state that, for $10° \leq \alpha \leq 66°$, the derived approximate expression for *z*(app) [Eq. (46)] is highly accurate since it produces maximum deviation sub-0.05%. Within this inclination angle range, the following can be written: (1) the approximation error is negligible from both a theoretical and practical standpoint; (2) the deviation is well below typical experimental uncertainty and modelling tolerances; and (3) the advocated method provides an excellent explicit substitute for the implicit fixed-point solution.

Furthermore, even for larger angles, the approximation remains robust and monotonic, with errors that are small and well-controlled, confirming the soundness of the underlying analytical development.

From a practical perspective, Fig. 3 supports the following recommendations:

1. **Preferred range**

For most hydraulic designs involving trapezoidal channels, inclination angles in the range $10° \leq \alpha \leq 65°$, should be preferred when using the proposed explicit formulation, as it guarantees near-exact results with minimal computational effort.

2**. Steep sidewalls ($\alpha > 65°$)**

For very steep channel sides, the approximation may still be employed safely for preliminary design and sensitivity analyses. However, for high-precision studies, it may be advisable to either revert to the implicit fixed-point solution, or apply a corrective factor based on the observed deviation trend.

3. **Design implication**

The presence of a minimum deviation around $\alpha \approx 45°$ (Fig. 3) highlights this inclination as particularly favorable from both a hydraulic and numerical standpoint, combining geometric efficiency with excellent predictive accuracy.

A one-shot accelerated fixed-point approximation

Presentation of the method

In this section, a second strong and accurate approximation, different in nature from the controlled cube-root linearization developed earlier, is to use a closed-form Aitken-Steffensen acceleration applied to the fixed-point form of the implicit governing Eq. (12). This produces a non-iterative "one-shot" estimate after only two substitutions into the fixed-point map, and it is especially effective when the fixed-point iteration is already contractive.

The Aitken–Steffensen acceleration provides a powerful and mathematically rigorous alternative for constructing an explicit approximation of the implicit normal-flow depth governing equation. The method is rooted in convergence theory and exploits the strong contractive nature of the fixed-point formulation associated with the Darcy-Weisbach-RMM framework. Instead of modifying the structure of the governing equation, the approach operates directly on the fixed-point mapping itself, making it fully consistent with the original physical model.

The central idea is to transform a slowly convergent iterative sequence into a rapidly convergent, or effectively non-iterative, estimate by analytically cancelling the dominant error component. When a fixed-point iteration converges, the error in successive iterates decreases approximately in a geometric manner. The Aitken-Steffensen technique takes explicit advantage of this property by combining only two successive updates of the fixed-point operator to extrapolate the limit of the sequence. In doing so, it suppresses the leading-order error term without requiring knowledge of the contraction factor or any derivative information.

Applied to the implicit normal-flow depth Eq. (12), this acceleration yields a genuine one-shot explicit approximation. Starting from a physically reasonable initial estimate, such as especially the improved Eq. (13), only two evaluations of the fixed-point operator are required to obtain a highly accurate approximation of the true solution. No convergence tolerance, iteration loop, or stopping criterion is needed. The resulting estimate is therefore computationally inexpensive, fully deterministic, and easy to implement.

A key strength of this method is that it does not rely on asymptotic simplifications or empirical fitting. Its accuracy stems directly from the mathematical structure of the fixed-point iteration and the smoothness of the governing nonlinear operator. Because the implicit normal-flow depth equation exhibits robust contraction over the entire domain of practical interest, the accelerated approximation remains stable and accurate for a wide range of relative conductivities and channel geometries. In particular, for moderate wall inclinations, the acceleration recovers the fixed-point solution with near-machine precision.

From a practical standpoint, the Aitken-Steffensen accelerated approximation offers an ideal compromise between analytical fidelity and numerical efficiency. It preserves the full physical content of the implicit formulation while eliminating the need for iterative solvers. This makes the method especially attractive for engineering calculations, parametric analyses, and embedded numerical implementations where both reliability and computational speed are essential.

In short, the accelerated fixed-point approximation represents a natural and rigorous extension of the iterative framework. It complements the controlled analytical explicit approximation developed elsewhere in the study and further strengthens the case for replacing traditional empirical approaches with physically consistent and mathematically sound tools for normal-flow depth computation in trapezoidal channels.

Model derivation

Starting from Eq. (19) recalled as follows:

$$z = \Phi\left(z\right) \tag{19}$$

one may then use the following iteration to approximate the solution:

$$z_{n+1} = \Phi\left(z_n\right) \tag{47}$$

Thus, we assume we have a fixed-point map Φ, given by Eq. (12), and the true solution z satisfies Eq. (19).

Thus, let the true solution be z. Define the absolute error in z at step n as follows:

$$e_n = z_n - z \tag{48}$$

Then, the following can be written:

$$z_n = z + e_n \tag{49}$$

Because:

$$z_{n+1} = \Phi\left(z_n\right) \tag{47}$$

and

$$z = \Phi\left(z\right) \tag{19}$$

one may write what follows:

$$z_{n+1} - z = \Phi\left(z_n\right) - \Phi\left(z\right) \tag{50}$$

From Eq. (48), this can be translated as follows:

$$e_{n+1} = \Phi\left(z_n\right) - \Phi\left(z\right) \tag{51}$$

On the other hand, when a fixed-point iteration converges, it is well known that near the solution the error behaves approximately like a geometric progression as follows:

$$e_{n+1} \approx \lambda e_n \tag{52}$$

where λ is a constant contraction factor with $|\lambda| < 1$.

This is not an arbitrary assumption: it is exactly what happens when the map Φ is smooth and the iteration is sufficiently close to the fixed point; then λ is essentially the derivative $\Phi'(z)$.

Consequently, let's use the following:

$$e_1 \approx \lambda e_0 \tag{53}$$

$$e_2 \approx \lambda e_1 = \lambda^2 e_0 \tag{54}$$

Eq. (49) allows writing the following:

$$z_0 = z + e_0 \tag{55}$$

$$z_1 = z + e_1 \tag{56}$$

$$z_2 = z + e_2 \tag{57}$$

Nos, let's compute the following first difference:

$$\Delta z_0 = z_1 - z_0 = \left(z + e_1\right) - \left(z + e_0\right) = e_1 - e_0 \tag{58}$$

Using Eq. (53), Eq. (58) reduces to the following:

$$\Delta z_0 \approx \lambda e_0 - e_0 = \left(\lambda - 1\right)e_0 \tag{59}$$

Now, let's compute the second difference as follows:

$$\Delta z_1 = z_2 - z_1 = \left(z + e_2\right) - \left(z + e_1\right) = e_2 - e_1 \tag{60}$$

Using Eqs. (53) and (54), Eq. (60) becomes as follows:

$$\Delta z_1 \approx \lambda^2 e_0 - \lambda e_0 = \lambda(\lambda - 1)e_0 \tag{61}$$

Now let's compute the difference of differences, i.e., the second finite difference, as follows:

$$\Delta^2 z_0 = \Delta z_1 - \Delta z_0 \tag{62}$$

Substituting the approximations expressed by Eqs. (59) and (61) into Eq. (62) yields the following:

$$\Delta^2 z_0 \approx \lambda(\lambda - 1)e_0 - (\lambda - 1)e_0 \tag{63}$$

Eq. (63) can be written in the following final form:

$$\Delta^2 z_0 \approx (\lambda - 1)^2 e_0 \tag{64}$$

From Eq. (59), one may derive the following:

$$e_0 \approx \frac{\Delta z_0}{\lambda - 1} \tag{65}$$

On the other hand, Eq. (59) provided what follows:

$$\left(\Delta z_0\right)^2 \approx (\lambda - 1)^2 e_0^2 \tag{66}$$

Dividing Eq. (66) by Eq. (64) yields the following:

$$\frac{\left(\Delta z_0\right)^2}{\Delta^2 z_0} \approx \frac{(\lambda - 1)^2 e_0^2}{(\lambda - 1)^2 e_0} = e_0 \tag{67}$$

This allows deriving the following:

$$e_0 \approx \frac{\left(\Delta z_0\right)^2}{\Delta^2 z_0} \tag{67a}$$

Substituting Eq. (67a) into Eq. (55) yields what follows:

$$z \approx z_0 - \frac{\left(\Delta z_0\right)^2}{\Delta^2 z_0} \tag{68}$$

In addition, for any sequence

$$\{z_n\}$$

the first forward difference at index n is defined by the following:

$$\Delta z_n = z_{n+1} - z_n \tag{69}$$

Thus, in particular, one may write the following:

At $n = 0$

$$\Delta z_0 = z_1 - z_0 \tag{70}$$

At $n = 1$

$$\Delta z_1 = z_2 - z_1 \tag{71}$$

The second forward difference is defined as the difference of the first differences as follows:

$$\Delta^2 z_n = \Delta z_{n+1} - \Delta z_n \tag{72}$$

Thus:

at $n = 0$

$$\Delta^2 z_0 = \Delta z_1 - \Delta z_0 \tag{73}$$

Substituting Eqs. (70) and (71) into Eq. (73) yields the following:

$$\Delta^2 z_0 = \left(z_2 - z_1\right) - \left(z_1 - z_0\right) \tag{74}$$

Expanding Eq. (74) results in the following:

$$\Delta^2 z_0 = z_2 - 2z_1 + z_0 \tag{75}$$

Substituting Eqs. (70) and (75) into Eq. (68), the following final relationship is obtained:

$$z(\text{app}) \approx z_0 - \frac{\left(z_1 - z_0\right)^2}{z_2 - 2z_1 + z_0} \tag{76}$$

It is useful to recall the following:

$$z_0 = \frac{1}{4} + \left(2\sqrt{1+m^{-2}}\right)^{2/5} \left(Q^*\right)^{4/5} \tag{13}$$

$$z_1 = \frac{1}{4} + \left(Q^*\right)^{2/3} \left[1 + \left(2\sqrt{z_0} - 1\right)\sqrt{1+m^{-2}}\right]^{1/3} \tag{12a}$$

$$z_2 = \frac{1}{4} + \left(Q^*\right)^{2/3} \left[1 + \left(2\sqrt{z_1} - 1\right)\sqrt{1+m^{-2}}\right]^{1/3} \tag{12b}$$

Using the last three relationships, Eq. (76) provides the sought value of the reduced normal flow depth z.

Fig. 4 illustrates the maximum relative deviation in the reduced normal flow depth z, expressed in percent, obtained when the Aitken-Steffensen accelerated approximation, expressed by Eq. (76), is used to solve the implicit governing Eq. (12) for trapezoidal open channels. The deviation is evaluated over the entire relative conductivity range $0.1 \leq Q^* \leq 4$, and is presented as a function of the sidewall inclination angle α.

This deviation reflects the discrepancy between the accelerated one-shot approximation and the reference solution obtained from the exact the exact implicit governing Eq. (12). As such, it provides a direct and meaningful measure of the global accuracy of the Aitken-Steffensen approach across both hydraulic and geometric parameters.

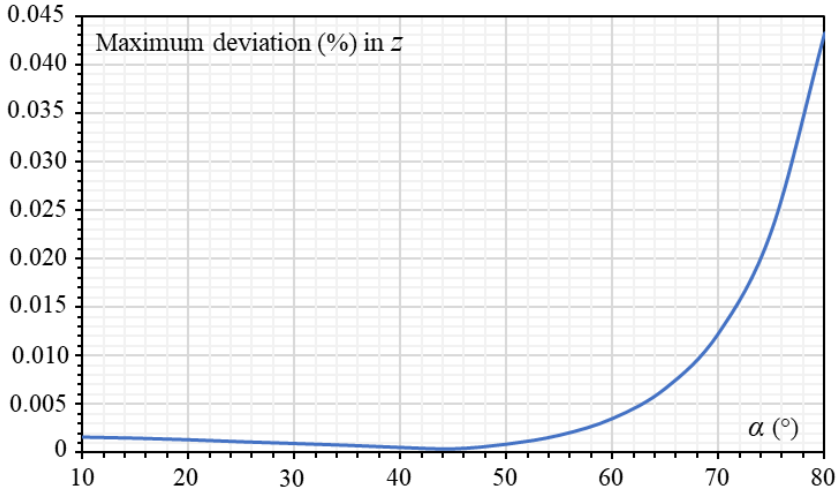

Figure 4: Maximum deviation (%) in z produced by Eq. (76), compared with the exact implicit governing Eq. (12), with respect to the inclination angle α (°), within the full rang $0.1 \leq Q^* \leq 4$

Fig. 4 reveals a smooth and well-structured dependence of the approximation error on the inclination angle, such that: (1) For moderate sidewall inclinations, approximately $10° \leq \alpha \leq 62°$, the maximum deviation remains extremely small, clearly sub-0.005 % and often close to the numerical resolution of the calculations. This demonstrates that, within this range, the Aitken-Steffensen approximation reproduces the exact implicit solution with quasi-exact accuracy for all values of $Q*$ considered; (2) A minimum deviation is observed around $\alpha \approx 44°$, indicating an optimal geometric configuration in which the fixed-point map is most nearly linear in the vicinity of the solution. In this case, the error cancellation mechanism underlying the Aitken-Steffensen procedure is particularly effective; and (3) For steeper channel sides, corresponding to $\alpha > 63°$, the deviation increases gradually and then more rapidly as α approaches 80°, reaching a maximum of about 0.043 %. This growth reflects the increasing nonlinearity of the governing equation as the geometric parameter

$$\sqrt{1 + m^{-2}}$$

becomes large. Nevertheless, even in this extreme range, the maximum deviation remains remarkably small.

In addition, several important conclusions can be drawn from Fig. 4.

1. High reliability over practical geometries

For sidewall inclinations commonly encountered in engineering practice, i.e., $\alpha \leq 55°$-60°, the Aitken-Steffensen accelerated solution is effectively exact, with deviations far below practical design tolerances.

2. Excellent global behavior

The absence of oscillations or abrupt changes confirms the smoothness and stability of the accelerated approximation over the entire geometric range.

3. Robustness for steep sidewalls

Even under extreme geometric conditions, the method maintains maximum relative deviation well below 0.05 %, confirming its suitability for preliminary design and analytical studies involving steep trapezoidal sections.

4. Complementarity with iterative schemes

The figure demonstrates that the Aitken-Steffensen procedure provides a fast and accurate alternative to fully iterative solvers, while remaining fully consistent with the underlying fixed-point formulation.

On the other side, it is worth noting that, fom a practical standpoint, the Aitken-Steffensen accelerated approximation can be confidently recommended as a non-iterative solution for normal-flow depth computation in trapezoidal channels, particularly when rapid evaluation is required, embedded or repetitive computations are performed, or an explicit yet highly accurate estimate is preferred.

In addition, for very steep sidewalls, the approximation remains reliable; however, if exceptionally higher accuracy is required, the user may optionally perform one additional fixed-point iteration.

Qualitative resemblance between Figs. 3 and 4 - interpretation and significance

Although Figs. 3 and 4 are obtained using two distinct approximation strategies, namely the controlled analytical linearization for Fig. 3 and the Aitken-Steffensen accelerated fixed-point approximation for Fig. 4, they exhibit a clear and striking qualitative resemblance in both overall shape and behavioral trends. This resemblance is neither accidental nor superficial; rather, it reflects a deeper mathematical and physical consistency inherent in the underlying implicit governing equation.

In both figures, the maximum deviation in the reduced normal flow depth z displays a smooth, unimodal evolution with respect to the sidewall inclination angle α. In particular, three common qualitative features are observed: (1) Very small deviations for moderate inclination angles, (2) The presence of a minimum deviation around intermediate angles, close to $\alpha \approx 40° - 45°$, and (3) A progressive increase in the maximum deviation for steep sidewalls, as approaches 80°.

This shared behavior confirms that both approximation methods are governed by the same fundamental source of nonlinearity: the geometric contribution of the sidewall inclination embedded in the implicit equation through the combined square-root and cube-root terms. As α increases, this geometric contribution amplifies the sensitivity of the solution, leading to a gradual deterioration in approximation quality, an effect captured by both methods in an analogous manner.

The quantitative difference between Figs. 3 and 4, however, reflects the distinct mathematical mechanisms by which each approximation operates. The controlled analytical approximation (Fig. 3) relies on a local linearization about a carefully selected reference state. Its accuracy therefore depends primarily on how well this reference state captures higher-order nonlinear effects, particularly for steep geometries. In contrast, the Aitken-Steffensen accelerated approximation (Fig. 4) directly exploits the contractive nature of the fixed-point mapping itself. By cancelling the dominant error component associated with geometric convergence, this method naturally achieves a lower maximum deviation across the entire inclination range.

Despite this quantitative improvement, the fact that both curves share the same qualitative structure is highly significant. It indicates that the error behavior is fundamentally dictated by the geometry of the trapezoidal section, not by the approximation technique. In other words, the governing equation itself imprints a characteristic response pattern with respect to α, and any physically consistent approximation, regardless of its analytical construction, will necessarily reflect this pattern.

From a methodological standpoint, this resemblance provides strong mutual validation of both approaches. It confirms that: (1) the controlled analytical approximation captures the

correct leading-order physics of the problem, and (2) the Aitken-Steffensen acceleration refines, rather than alters, this underlying behavior.

Thus, the two figures should not be viewed as competing results, but rather as complementary representations of the same mathematical reality, with Fig. 4 offering a quantitatively sharper realization of a trend already correctly identified in Fig. 3.

Newton's method on a single scalar equation

In this section, we develop an accurate method which is not "fixed-point iteration"; it is Newton's method applied to the implicit governing Eq. (12) itself. For smooth hydraulic problems like Eq. (12), Newton's method converges very rapidly as it requires often 1 to 2 steps with a reasonable starting guess such as especially Eq. (13).

Let's define the same notation as earlier:

$$\omega = \left(Q^*\right)^{2/3} \tag{16}$$

$$s = \sqrt{1 + m^{-2}} \tag{17}$$

$$B(z) = 1 + s\left(2\sqrt{z} - 1\right) \tag{31}$$

Thus, the implicit governing Eq. (12) is equivalent to the following:

$$z = \frac{1}{4} + \omega\left[B(z)\right]^{1/3} \tag{77}$$

Let's bring all terms to one side such as writing what follows:

$$F(z) = z - \frac{1}{4} - \omega\left[B(z)\right]^{1/3} = 0 \tag{78}$$

Taking into account Eq. (42), the following derivative can be written:

$$F'(z) = 1 - \frac{1}{3}\omega\left[B(z)\right]^{-2/3}\frac{s}{\sqrt{z}} \tag{79}$$

The well-known Newton's method is written as follows:

$$z_{k+1} = z_k - \frac{F\left(z_k\right)}{F'\left(z_k\right)} \tag{80}$$

Substituting Eqs. (78) and (79) into Eq. (80) results in the following final relationship:

$$z_{k+1} = z_k - \frac{z_k - \frac{1}{4} - \omega\left[B\left(z_k\right)\right]^{1/3}}{1 - \frac{1}{3}\omega\left[B\left(z_k\right)\right]^{-2/3}\frac{s}{\sqrt{z_k}}} \tag{81}$$

One-step approximation and accuracy

The one-step approximation using Eq. (81) is obtained for $k = 0$, so that writing Eq. (81) as follows:

$$z(\text{app}) = z_1 = z_0 - \frac{z_0 - \frac{1}{4} - \omega\left[B\left(z_0\right)\right]^{1/3}}{1 - \frac{1}{3}\omega\left[B\left(z_0\right)\right]^{-2/3}\frac{s}{\sqrt{z_0}}} \tag{82}$$

It is useful to recall the following:

$$\omega = \left(Q^*\right)^{2/3} \tag{16}$$

$$s = \sqrt{1 + m^{-2}} \tag{17}$$

$$z_0 = \frac{1}{4} + \left(Q^*\right)^{4/5}(2s)^{2/5} \tag{30}$$

$$B\left(z_0\right) = B_0 = 1 + s\left(2\sqrt{z_0} - 1\right) \tag{43}$$

Fig. 5 presents the distribution of the maximum relative deviation (%) in the reduced normal flow depth z produced by a single Newton update, as expressed by Eq. (82), over the entire relative conductivity range $0.1 \leq Q* \leq 4$, plotted as a function of the trapezoidal channel sidewall inclination angle α (°). This figure provides valuable insight into the behavior of Newton's method when it is deliberately restricted to a one-step computation, thereby allowing a direct and meaningful comparison with the other approximation strategies investigated in this study.

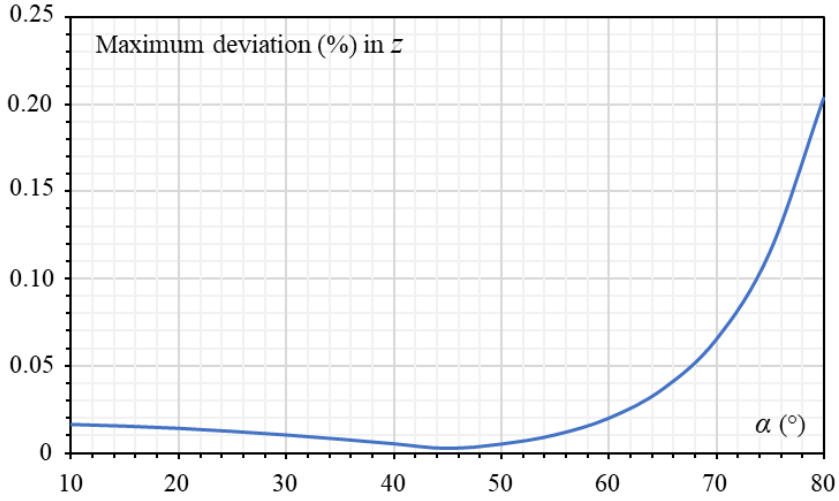

Figure 5: Maximum deviation (%) in z produced after the one-step computation using the Newton's method expressed by Eq. (82), with respect to the inclination angle α (°), within the full range $0.1 \leq Q^* \leq 4$

A first and important observation is that Fig. 5 exhibits a clear qualitative resemblance to Figs. 2, 3, and 4. In all cases, the maximum deviation displays a smooth, unimodal dependence on the inclination angle α, characterized by three recurring features: (1) very small deviations for moderate channel wall inclinations, (2) the presence of an optimal angular range where the deviation reaches a minimum, and (3) a progressive increase in deviation as the sidewalls become steep and approach the vertical configuration.

This similarity in shape and trend is not coincidental. It reflects the fact that all methods, fixed-point iteration (Fig. 2), controlled analytical approximation (Fig. 3), Aitken-Steffensen acceleration (Fig. 4), and one-step Newton correction (Fig. 5), are ultimately governed by the same intrinsic nonlinearity embedded in the implicit governing Eq. (12). In particular, the combined influence of the square-root and cube-root terms amplifies the sensitivity of the solution as the geometric parameter associated with α increases. Consequently, any physically consistent approximation scheme will naturally reproduce the same qualitative response with respect to wall inclination.

From a quantitative standpoint, however, Fig. 5 reveals a behavior that is distinct and instructive. Compared with Fig. 4, the deviations produced by the one-step Newton method are generally larger, comparable however to Fig. 3, especially for moderate to steep inclinations. This outcome is entirely consistent with the mathematical nature of Newton's method: while it possesses quadratic convergence in the vicinity of the exact solution, its accuracy after a single iteration depends critically on how close the initial guess is to the true root. In the present formulation, the initial guess is chosen to be general and robust rather than specifically optimized for Newton's method, which explains why a single Newton step does not fully exploit the method's potential convergence rate.

Nevertheless, the maximum deviations shown in Fig. 5 remain well-controlled and smooth across the entire angular range. For moderate inclinations, particularly within the interval $10° \leq \alpha \leq 60°$, the one-step Newton approximation already yields deviations that are acceptable for many practical engineering applications (Sub-0.02%). As α increases beyond this range, the deviation grows more rapidly than in Figs. 3 and 4, illustrating that Newton's method, when truncated after one iteration, is more sensitive to geometric nonlinearity than either the controlled analytical approximation or the Aitken-Steffensen accelerated scheme.

The qualitative resemblance between Fig. 5 and the other figures carries important methodological implications. It confirms that the implicit governing equation itself dictates the global error structure, while the chosen numerical or analytical method determines only the magnitude of that error. In this sense, Fig. 5 reinforces the interpretation already drawn from Figs. 3 and 4: the error pattern is geometry-driven, whereas the relative performance of each method is dictated by how effectively it captures or mitigates the dominant nonlinear terms of the original implicit equation.

From a practical perspective, Fig. 5 suggests that while Newton's method is theoretically powerful, its use as a one-step explicit approximation is less attractive than the alternatives proposed in the study. To achieve accuracy comparable to that shown in Fig. 4, Newton's method would require additional iterations, derivative evaluations, and careful numerical handling, thereby forfeiting its simplicity advantage. By contrast, the controlled analytical approximation (Achour and Amara model) and the Aitken-Steffensen acceleration achieve superior accuracy with minimal computational effort and without repeated derivative calculations.

In conclusion, Fig. 5 plays a complementary role within the study. It demonstrates that even a single Newton update reproduces the correct qualitative behavior of the solution and confirms the robustness of the initial guess. However, when compared with Fig. 4, it also highlights why Newton's method is not the most efficient or practical choice for this problem. The comparison underscores the central message of the paper: although different solution techniques may share the same qualitative behavior due to the intrinsic structure of the governing equation, carefully designed fixed-point and explicit approximation strategies provide a far more balanced combination of accuracy, robustness, and computational efficiency for normal-flow depth computation in trapezoidal channels.

Two-step approximation and accuracy

If user needs higher accuracy than that illustrated in Fig. 5, especially for steeper sidewalls, an additional computation step is then required. The additional step can be translated into the following relationship, coming from Eq. (81) for $k = 1$ as follows:

$$z(\text{app}) = z_2 = z_1 - \frac{z_1 - \frac{1}{4} - \omega\left[B(z_1)\right]^{1/3}}{1 - \frac{1}{3}\omega\left[B(z_1)\right]^{-2/3}\frac{s}{\sqrt{z_1}}} \tag{83}$$

Evidently, z_1 is given by Eq. (82). Let's specify the following:

$$\omega = \left(Q^*\right)^{2/3} \tag{16}$$

$$s = \sqrt{1 + m^{-2}} \tag{17}$$

$$B(z_1) = B_1 = 1 + s\left(2\sqrt{z_1} - 1\right) \tag{84}$$

Fig. 6 illustrates the distribution of the maximum relative deviation (in percent) of the reduced normal flow depth z obtained using the two-step Newton approximation, denoted $z(\text{app}) = z_2$, with respect to the trapezoidal channel sidewall inclination angle α expressed in degree. For each value of α, the deviation shown corresponds to the maximum relative error observed over the full relative conductivity range $0.1 \le Q^* \le 4$. The inclination angle is varied continuously between 10°and 80°. The maximum deviation is computed relative to the reference solution obtained from the exact implicit governing Eq. (12).

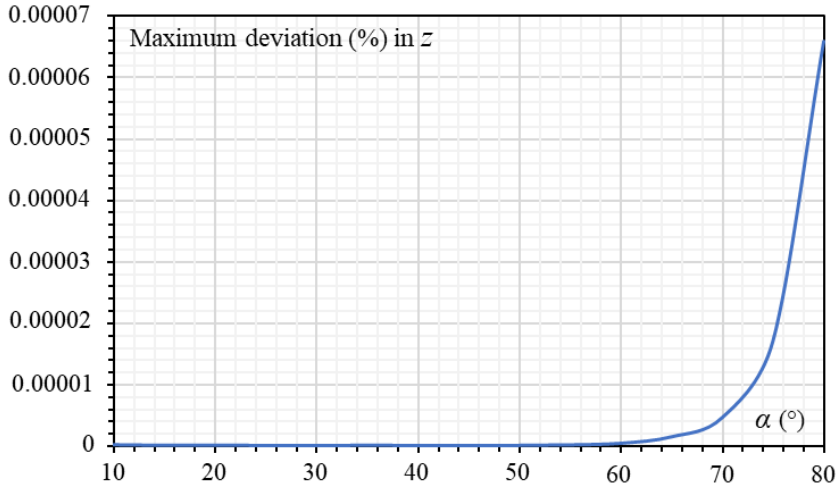

Figure 6: Maximum deviation (%) in z produced after the two-step computation using the Newton's method expressed by Eq. (83), with respect to the inclination angle α (°), within the full range $0.1 \le Q^* \le 4$

The most striking feature of the figure is the **e**xtremely small magnitude of the deviations over almost the entire range of inclination angles. For moderate wall inclinations,

approximately $10° \leq \alpha \leq 65°$, the maximum deviation is practically negligible, remaining well below 10^{-5} %. This indicates that, within this broad and practically relevant interval, the solution produced after only two Newton iterations is virtually indistinguishable from the fully converged solution.

As the inclination angle increases beyond about 65°, a gradual rise in deviation becomes noticeable, followed by a sharper increase as α approaches 80°. Even in this extreme geometric regime, however, the maximum deviation remains exceptionally small, sub-0.00007 %. Such error levels are far below any practical engineering tolerance and demonstrate the remarkable efficiency and robustness of the two-step Newton method when applied to the implicit governing equation.

From a qualitative standpoint, the curve shown in Fig. 6 exhibits a shape and trend that are consistent with those observed in Figs. 2, 3, and 4. In all cases, the error evolves smoothly with the inclination angle, showing minimal deviation for moderate values of α and increasing progressively for steep channel sidewalls. This common behavior confirms that the geometry-induced nonlinearity embedded in the governing equation controls the global structure of the error, independently of the solution method employed.

The fundamental difference lies in the magnitude of the maximum deviation. While the fixed-point scheme, the controlled analytical approximation, and the Aitken-Steffensen acceleration each introduce small but measurable errors, the two-step Newton method reduces these errors by several orders of magnitude. This dramatic improvement is consistent with the quadratic convergence property of Newton's method once the solution lies sufficiently close to the true root, a condition already satisfied by the carefully chosen initial guess expressed by Eq. (13).

Fig. 6 clearly demonstrates that performing only two Newton iterations provides an almost exact solution of the implicit governing equation over the entire investigated domain. In practical terms, this means that: (1) the two-step Newton method offers near-machine-precision accuracy with minimal computational effort; (2) it represents an ideal compromise between simplicity and accuracy; and (3) for engineering design and analysis, further iterations offer no tangible benefit.

In other words, Fig. 6 provides compelling evidence that the two-step Newton method is among the most accurate and reliable solution strategies examined in the study. It not only preserves the qualitative behavior dictated by the governing equation but also achieves a level of accuracy that effectively renders the solution exact for practical purposes. Within the context of the present work, it establishes the two-step Newton scheme as a benchmark against which other approximate and explicit methods can be objectively assessed. However, it is emphasis to note that other developed previous approximate relationships, such as Eq. (76), could also provide such small deviations when the two-step computation is applied.

An accurate derivative-free secant one-shot approximation

Presentation of the approximate model

The derivative-free secant approximation constitutes a robust, simple, and highly accurate alternative for solving the implicit governing equation of the reduced normal flow depth. Unlike Newton-type methods, which require explicit differentiation of the nonlinear operator, this approach is built entirely on function evaluations of the governing equation itself, thereby eliminating the need for analytical derivatives while preserving fast convergence characteristics.

The method is based on the classical secant method, a root-finding technique that approximates the local slope of a nonlinear residual function by a finite difference computed from two nearby trial values. When applied to the implicit normal-flow depth Eq. (12), the secant approach exploits the smoothness and monotonicity of the residual function arising from the Darcy-Weisbach-RMM formulation. These properties ensure numerical stability and a strong tendency toward rapid convergence, even when the solution is obtained in a single update.

In the present context, the implicit governing equation is first reformulated as a scalar residual equation whose root corresponds to the desired reduced normal flow depth. Two explicit trial values are then introduced. The first, i.e., z_0, is a physically consistent initial estimate derived from the asymptotic behavior of the governing equation, which captures the dominant hydraulic scaling across the entire relative conductivity range; To do so, the appropriate initial guess relationship expressed by Eqs. (13) or (30) will be adopted. The second trial value, i.e. z_1 expressed by Eq. (12a), is obtained by a single direct substitution of this estimate into the implicit equation itself. These two values provide the necessary information to approximate the local slope of the residual function without differentiation.

Using this finite-difference slope, a single secant update is performed to extrapolate the location of the root. The resulting approximation is fully explicit and requires only two evaluations of the residual function. No convergence tolerance, stopping criterion, or iteration loop is involved, making the method computationally efficient and straightforward to implement.

The accuracy of the derivative-free secant approximation stems from its ability to locally emulate the behavior of Newton's method while avoiding its algebraic complexity. Because the implicit governing equation is smooth and well behaved over the entire range of relative conductivities and sidewall inclinations considered, the secant update effectively cancels the leading-order error component associated with the initial estimate. As a result, the approximation often achieves an accuracy comparable to accelerated fixed-point schemes and, in many practical cases, approaches that of a two-step Newton solution.

From a practical standpoint, this method offers an excellent compromise between simplicity and acceptable accuracy. It requires minimal computational effort, relies exclusively on physically meaningful quantities, and is easily implemented in spreadsheet

calculations or embedded engineering software. The derivative-free secant approximation therefore represents a valuable addition to the family of solution strategies proposed for the implicit normal-flow depth equation, complementing both the analytical explicit models and the Newton-based iterative approaches discussed elsewhere in the paper.

Approximate model formulation

The advocated model is simply written as follows:

$$z(\text{sec}) = z_1 - F(z_1)\frac{z_1 - z_0}{F(z_1) - F(z_0)} \tag{85}$$

where "sec" denotes "secant" with relating to the advocated method. All the terms of Eq. (85) have already been defined previously, in particular:

$$z_0 = \frac{1}{4} + \left(Q^*\right)^{4/5}(2s)^{2/5} \tag{30}$$

$$s = \sqrt{1 + m^{-2}} \tag{17}$$

$$z_1 = \frac{1}{4} + \omega\left[B(z_0)\right]^{1/3} \tag{77}$$

$$\omega = \left(Q^*\right)^{2/3} \tag{16}$$

$$B(z_1) = B_1 = 1 + s\left(2\sqrt{z_1} - 1\right) \tag{84}$$

$$F(z_1) = z_1 - \frac{1}{4} - \omega\left[B(z_1)\right]^{1/3} \tag{78a}$$

$$F(z_0) = z_0 - \frac{1}{4} - \omega\left[B(z_0)\right]^{1/3} \tag{78b}$$

$$B(z_0) = B_0 = 1 + s\left(2\sqrt{z_0} - 1\right) \tag{43}$$

Fig. 7 illustrates the distribution of the maximum relative deviation (in percent) of the reduced normal flow depth z obtained using the one-shot derivative-free secant approximation, as a function of the trapezoidal channel sidewall inclination angle α expressed in degree. For each inclination angle, the deviation shown corresponds to the maximum relative error observed over the complete relative conductivity domain $0.1 \leq Q^* \leq 4$. The inclination angle varies from 10° to 80°, covering both gently sloping and

steep trapezoidal channel configurations. The deviation is evaluated with respect to the reference solution obtained from the fully converged governing implicit Eq. (12).

The curve exhibits a smooth, monotonic evolution with respect to the inclination angle, characterized by very small maximum deviations at low and moderate values of α, followed by a progressively steeper increase as the sidewalls approach the vertical configuration. For angles roughly within the range $10° \leq \alpha \leq 62°$, the maximum deviation produced by the one-shot secant approximation remains extremely small, typically sub-0.005 %, i.e., well below engineering significance. This indicates that, in this inclination angle interval, the secant-based explicit estimate reproduces the implicit solution with high reliability over the entire range of relative conductivities considered.

As the inclination angle α increases beyond this range, the deviation begins to grow in a gradual and continuous manner, becoming more pronounced for α greater or equal to 65°. Near $\alpha = 80°$, the deviation reaches its maximum value, yet it remains bounded and relatively small. This increase reflects the enhanced nonlinearity of the governing equation for steep trapezoidal sections, where the geometric contribution associated with the sidewall inclination magnifies the sensitivity of the solution. As it was observed of the previous figures, the curve in Fig. 7 exhibits a minimum at about $\alpha = 45°$ where the physical interpretation stills the same.

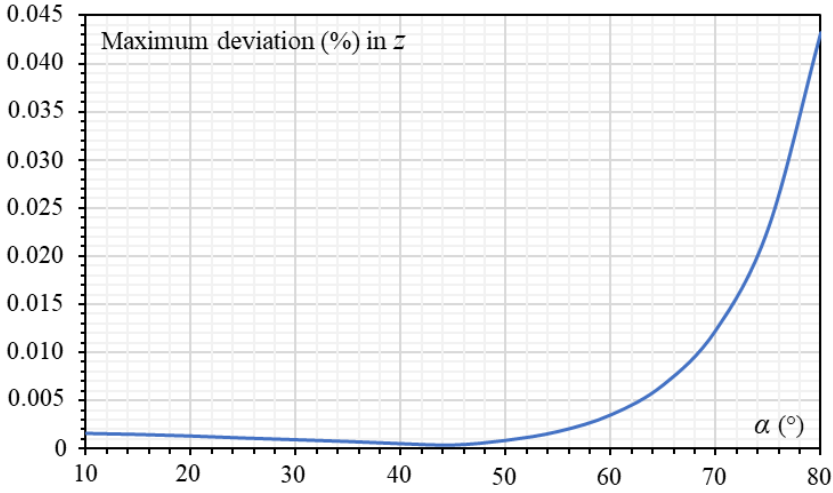

Figure 7: Distribution of the maximum deviation (%) in z produced by the one-shot secant approximation expressed by Eq. (85), with respect to the inclination angle α (°), within the full range $0.1 \leq Q^* \leq 4$

A salient feature of Fig. 7 is its strong qualitative resemblance to the maximum relative error distributions obtained using the other approximation strategies discussed earlier, including the controlled analytical approximation, the Aitken-Steffensen accelerated scheme, and the one-step Newton method. In all cases, the deviation curves share the same global structure: a near-flat region at low to moderate inclination angles, a minimum or plateau around intermediate values of α, and a sharp rise for steep sidewalls.

This consistent trend confirms that the overall behavior of the maximum relative error is primarily dictated by the intrinsic structure of the implicit governing equation, rather than by the particular numerical or analytical method employed. The sidewall inclination acts as the dominant parameter controlling the strength of the nonlinear terms, and any physically consistent approximation necessarily reflects this dependence.

Although the qualitative behavior is similar, the magnitude of the deviation differs quantitatively from that obtained using other methods. The one-shot secant approximation produces maximum relative errors that are larger than those obtained with the two-step Newton method or the Aitken-Steffensen acceleration, but comparable in order of magnitude to those observed for the controlled analytical approximation. This outcome is fully consistent with the derivative-free nature of the secant method: by replacing the exact derivative with a finite-difference approximation based on two trial points, the method achieves simplicity at the expense of some loss of accuracy.

Nonetheless, the deviation levels remain modest and well controlled over the entire range of α, demonstrating that the secant-based approximation strikes a favorable balance between computational simplicity and accuracy. Its performance is particularly satisfactory for the range of inclination angles most commonly encountered in practice, where the maximum deviation is minimal.

Fig. 7 confirms that the one-shot derivative-free secant approximation is a robust and reliable explicit solution strategy for the implicit normal-flow depth Eq. (12). While it does not match the extreme accuracy of multi-step Newton schemes, it faithfully reproduces the correct qualitative behavior and delivers acceptable quantitative accuracy with minimal computational effort. The close similarity of its maximum relative error trend to those of the other methods further reinforces the conclusion that all proposed approximations are grounded in the same physical and mathematical structure, differing mainly in their degree of refinement rather than in their fundamental behavior.

Midpoint-Taylor quadratic explicit approximation (MTQEA)

Presentation of the model

The Midpoint-Taylor Quadratic Explicit Approximation (MTQEA) is a simple, robust, but moderately accurate analytical model developed by the authors to solve the implicit governing equation of the reduced normal flow depth in trapezoidal channels. It is conceived to overcome the limitations observed in classical explicit linearization and in higher-order Taylor expansions performed about arbitrary reference states, while retaining full analytical transparency and computational efficiency.

The implicit governing Eq. (12) is characterized by a composite nonlinearity, combining a square-root dependence on the reduced flow depth and a cube-root dependence on a linear function of that square root. This nonlinear structure, while smooth and well behaved, leads to strong curvature effects that cannot be captured reliably by first-order approximations and may degrade the accuracy of higher-order Taylor expansions when they are performed far from the exact solution.

The MTQEA addresses this difficulty by embedding a predictor-corrector philosophy directly into a fully explicit analytical framework. Rather than expanding the nonlinear term around an a priori fixed reference state, such as initial guess, the method constructs a data-dependent expansion point that lies intrinsically close to the true solution. This key feature is what distinguishes the MTQEA from all other explicit models considered in the study.

The method proceeds in three logically distinct but computationally simple stages: (1) Predictor stage: A first explicit estimate of the reduced normal flow depth is generated using a closed-form expression derived from the dominant balance of the governing equation. This estimate is then injected once into the governing equation to obtain a corrected value through direct substitution. No iteration loop is involved; this single substitution is performed only once; (2) Midpoint reference selection: The arithmetic mean of the initial estimate and its corrected value is introduced as a reference state. This midpoint is not arbitrary: it lies between two physically admissible approximations and is therefore guaranteed to be closer to the exact solution than either value alone. In this sense, the reference state is automatically adapted to the hydraulic conditions and channel geometry under consideration; (3) Quadratic correction by second-order Taylor expansion: The cube-root term, which encapsulates the principal nonlinearity of the governing equation, is expanded to second order about the midpoint reference state. Because the argument of the cube-root is a linear function of the square-root of the relative flow depth, this expansion leads exactly to a quadratic algebraic equation in the auxiliary variable. Solving this quadratic yields a closed-form expression for the approximate solution, from which the reduced normal flow depth is obtained directly.

From a mathematical standpoint, the MTQEA exhibits several decisive strengths: (1) Local second-order accuracy near the solution, ensured by expanding the nonlinear operator about a dynamically chosen midpoint rather than a fixed reference, (2) Exact preservation of geometric dependence, since no approximation is introduced in the linear relation between geometry and the square-root variable, (3) Controlled truncation error, as the dominant curvature of the cube-root function is explicitly retained, and (4) Algebraic solvability, because the final equation is quadratic and admits a closed-form solution.

These properties explain why the MTQEA delivers accuracy comparable to multi-step Newton schemes while remaining explicit. However, as it will be seen in a next section, for $0.1 \leq Q^* \leq 4$, it is recommended for the following restricted inclination angle $10° \leq \alpha \leq 60°$, where the model produces a maximum deviation sub-0.1 %. The worst case occurs at $\alpha = 60°$

From a physical perspective, the MTQEA is firmly grounded in the hydraulic behavior of the system: (1) The predictor stage respects the correct asymptotic limits at both low and moderate relative conductivities, (2) The midpoint expansion point reflects the natural balance between geometric and relative conductivity effects, ensuring that the approximation remains physically admissible over the full considered domain, and (3) Sensitivity to extreme geometries, i.e., small inclination angles or steep sidewalls, is

strongly reduced, as demonstrated by the uniformly low deviations observed in numerical tests.

The method therefore adapts naturally to variations in relative conductivity and sidewall inclination without loss of stability.

Despite its acceptable accuracy, the MTQEA is computationally lightweight: (1) it requires only one evaluation of the governing equation, (2) it uses elementary operations, i.e., square roots, cube roots, and a quadratic formula, (3) it involves no iterative loops, convergence criteria, or derivative evaluations, and (4) it is easily implemented in spreadsheets, calculators, or embedded hydraulic codes.

This makes the method particularly attractive for practical engineering applications where simplicity and reliability are equally important.

The MTQEA occupies a unique position among the solution strategies considered for the implicit normal-flow depth equation. It is significantly more accurate than classical one-shot explicit linearization, yet far simpler than derivative-based or multi-iteration methods. By combining adaptive reference selection with a second-order analytical correction, it achieves a level of accuracy that was previously attainable only through iterative schemes.

As a concluding assessment, the Midpoint-Taylor Quadratic Explicit Approximation constitutes a powerful and elegant solution to the implicit governing equation of normal flow depth in trapezoidal channels, especially for $10° \leq \alpha \leq 60°$, Its construction is mathematically rigorous, physically well motivated, and computationally efficient. By capturing the essential nonlinear structure of the problem while remaining fully explicit, the MTQEA represents a compelling alternative to both traditional explicit formulas and more complex iterative methods.

Transformation of the governing implicit equation

Let's recall that the reduced normal flow depth z satisfies the implicit governing relationship expressed by Eq. (12). Let's also recall the following relationships that will be used in the present section:

$$\omega = \left(Q^*\right)^{2/3} \tag{16}$$

$$s = \sqrt{1 + m^{-2}} \tag{17}$$

Let's set what follows:

$$y = \sqrt{z}\,,\ y \geq 0 \tag{86}$$

Then Eq. (12) can be written equivalently as follows:

$$y^2 = \frac{1}{4} + \omega\left[1 + s\left(2y - 1\right)\right]^{1/3} \tag{87}$$

Let's define the following linear argument of the cube-root:

$$x\left(y\right) = 1 + s\left(2y - 1\right) = 1 - s + 2s\,y \tag{88}$$

Let's also define the following nonlinear term:

$$g\left(y\right) = \left[x\left(y\right)\right]^{1/3} \tag{89}$$

Then Eq. (87) becomes as follows:

$$y^2 = \frac{1}{4} + \omega\, g\left(y\right) \tag{90}$$

At this stage, the only nonlinear element in the equation is the cube-root dependence.

Note that for $\omega = 0$, Eq. (90) allows writing $y = 1/2$. Thus, for $\omega > 0$, y is greater than 1/2.

Appropriate initial guess relationship

We need an explicit reference value, i.e., guess value, to expand around. Let's construct it from the dominant balance of Eq. (88) for moderate/large Q^*, the same physics used to build asymptotic starters, but derived herein explicitly.

For large y, Eq. (88) is then dominated by $2sy$, hence, Eq. (88) becomes as follows:

$$x\left(y\right) \approx 2s\,y \tag{91}$$

Then, Eq. (89) becomes as follows:

$$g\left(y\right) = \left(2s\,y\right)^{1/3} \tag{92}$$

Inserting Eq. (92) into Eq. (90) and neglect the constant 1/4 compared to y^2 in the dominant regime, yields the following:

$$y^2 \approx \omega\left(2s\,y\right)^{1/3} \tag{93}$$

Let's rewrite Eq. (93) by grouping powers of y; Thus, the following can be written:

$$y^2 \approx \omega\left(2s\right)^{1/3} y^{1/3} \tag{94}$$

After rearranging, Eq. (94) reduces to the following:

$$y^{5/3} \approx \omega\left(2s\right)^{1/3} \tag{95}$$

Now, let's raise both sides of Eq. (95) to the power 3/5; Thus, the following can be written:

$$y \approx \omega^{3/5} \left(2s\right)^{1/5} \tag{96}$$

Using Eq. (16), Eq. (96) becomes as follows:

$$y \approx \left(Q^*\right)^{2/5} \left(2s\right)^{1/5} \tag{97}$$

To also match the exact limiting case $Q* \to 0 \Rightarrow z \to 1/4$ [Eq. (12)] $\Rightarrow y \to 1/2$ [Eq. (86)], let's define the following explicit reference value, i.e., the sought initial guess relationship:

$$y_0 \approx \frac{1}{2} + \left(Q^*\right)^{2/5} \left(2s\right)^{1/5} \tag{98}$$

The initial guess is known since the relative conductivity Q^* expressed by Eq. (9) and $s(m)$ given by Eq. (17) can be computed based on the required available data, as illustrating in the earlier numerical example.

Now compute one predictor value denoted:

$$y_1$$

by one direct substitution of the governing equation (90). It reads as follows:

$$y_1 = \sqrt{\frac{1}{4} + \omega g\left(y_0\right)} \tag{99}$$

This is not an iteration scheme; we do it once only.

On the other side, when considering both Eqs. (88) and (89), one may write the following:

$$g\left(y_0\right) = \left(1 - s + 2\,s\,y_0\right)^{1/3} \tag{100}$$

Now take the midpoint reference such as writing the following:

$$y_c = \frac{y_0 + y_1}{2} \tag{101}$$

This is the key improvement: y_c is typically much closer to the true solution than y_0, even when the relative conductivity Q^* is large or the inclination angle α is small.

Second-order Taylor expansion of g(y) about y_c

We approximate $g(y)$ by its second-order Taylor polynomial at $y = y_c$; thus, the following can be written:

$$g(y) \approx g_c + g'_c\left(y - y_c\right) + \frac{1}{2}g''_c\left(y - y_c\right)^2 \tag{102}$$

where

$$g_c = g\left(y_c\right) = \left(1 - s + 2\,s\,y_c\right)^{1/3} \tag{103}$$

$$g'_c = g'\left(y_c\right) = \frac{2\,s}{3}\left(1 - s + 2\,s\,y_c\right)^{-2/3} \tag{104}$$

$$g''_c = -\frac{8\,s^2}{9}\left(1 - s + 2\,s\,y_c\right)^{-5/3} \tag{105}$$

Convert the governing equation into a quadratic in y

Inserting the Taylor approximation expressed by Eq. (102) into Eq. (90) yields the following:

$$y^2 = \frac{1}{4} + \omega\left[g_c + g'_c\left(y - y_c\right) + \frac{1}{2}g''_c\left(y - y_c\right)^2\right] \tag{106}$$

Expanding what follows:

$$\left(y - y_c\right)^2 = y^2 - 2yy_c + y_c^2 \tag{107}$$

After grouping terms, Eq. (106) becomes as follows:

$$A\,y^2 + B\,y + C = 0 \tag{108}$$

with the following explicit coefficients:

$$A = 1 - \frac{\omega}{2}g''_c \tag{109}$$

$$B = -\omega\,g'_c + \omega\,g''_c\,y_c \tag{110}$$

$$C = -\frac{1}{4} - \omega\,g_c + \omega\,g'_c\,y_c - \frac{\omega}{2}g''_c\,y_c^2 \tag{111}$$

Explicit solution and final z (app)

Solving the quadratic Eq. (108) results in the following real root:

$$y(\text{app}) = \frac{-B + \sqrt{B^2 - 4AC}}{2A} \tag{112}$$

The "+" root is the physically relevant one because it satisfies the condition:

$$y \geq 1/2$$

Finally, according to Eq. (86), the explicit approximate relationship governing the reduced normal flow depth z (app) is written as follows:

$$z(\text{app}) = \left(\frac{-B + \sqrt{B^2 - 4AC}}{2A} \right)^2 \tag{113}$$

Relative deviation (%) produced by the MTQEA

Fig. 8 illustrates the maximum relative deviation (in percent) of the reduced normal flow depth z obtained using the Midpoint-Taylor Quadratic Explicit Approximation (MTQEA), expressed by Eq. (113), as a function of the trapezoidal channel sidewall inclination angle α expressed in degree. For each value of α, the deviation shown corresponds to the maximum relative error observed over the entire relative conductivity range $0.1 \leq Q^* \leq 4$, when compared with the exact values provided by the exact implicit governing Eq. (12).

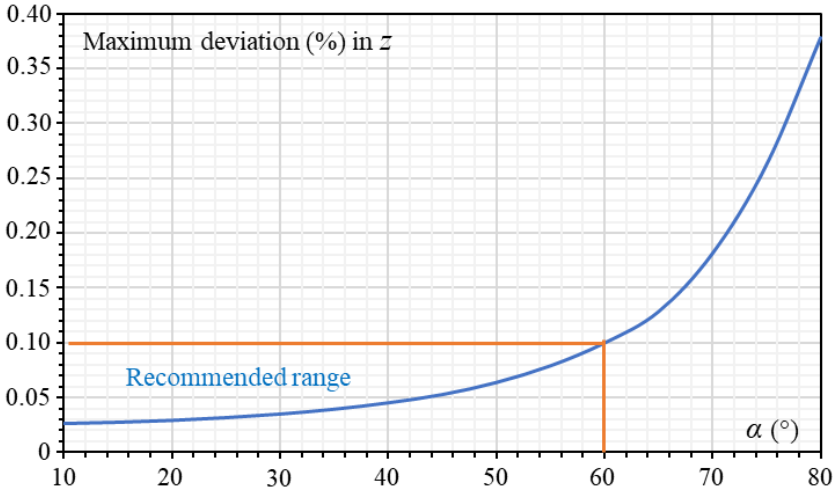

Figure 8: Distribution of the maximum deviation (%) in z produced by the MTQEA model expressed by Eq. (113), with respect to the inclination angle α (°), within the full range $0.1 \leq Q^* \leq 4$

The inclination angle is varied between 10° and 80°, thereby encompassing both gently sloping and steep sidewall configurations typically encountered in engineering practice.

The highlighted "recommended range" in the figure identifies the range of inclination angles for which the MTQEA yields its lowest and most stable maximum deviations.

Fig. 8 shows that the maximum deviation produced by the MTQEA remains remarkably small for moderate inclination angles and increases progressively as the sidewalls become steeper. For α values approximately between 10° and 60°, the maximum deviation remains below about 0.1%, indicating that within this range the MTQEA provides an exceptionally accurate approximation of the implicit governing equation over the full relative conductivity domain.

Beyond $\alpha = 60°$, the deviation begins to grow more rapidly, reflecting the increasing geometric sensitivity of the governing equation for steep trapezoidal sections. In this regime, the contribution of the sidewalls to the hydraulic geometry becomes dominant, and the nonlinear coupling between the reduced flow depth and the geometric parameter intensifies. As a result, even a second-order Taylor-based explicit correction, such as that employed by the MTQEA, gradually loses some of its effectiveness.

Nevertheless, it is important to emphasize that even for large inclination angles approaching 80°, the deviations remain bounded and relatively modest in absolute terms. This confirms the overall robustness of the MTQEA and its suitability for a wide range of geometries.

The "recommended area" identified in the figure corresponds to the interval of inclination angles for which the MTQEA achieves uniformly minimal deviation, both in magnitude and in sensitivity to changes in relative conductivity. This range is not chosen arbitrarily; it reflects a domain in which the intrinsic nonlinearity of the governing equation is naturally balanced by the channel geometry. In this configuration, the midpoint-based expansion on which the MTQEA is built remains very close to the exact solution, thereby minimizing truncation error.

From a practical perspective, this recommended range coincides with sidewall inclinations that are commonly used in trapezoidal channel design due to their favorable structural and hydraulic properties. Consequently, the MTQEA is not only accurate in an abstract mathematical sense, but also highly effective under conditions of real engineering relevance. Fig. 8 confirms once again that the dependence of the relative error on the inclination angle is a structural feature of the governing equation, rather than a peculiarity of a specific approximation technique.

In short, the figure clearly demonstrates that the MTQEA is a reliable, accurate, and practically oriented approximation method for solving the implicit normal-flow depth governing equation. The recommended area highlighted in the figure provides clear guidance for practitioners: within this range of sidewall inclinations, the MTQEA can be used with high confidence, delivering near-exact results without iteration. Even outside this range, the method remains robust and predictable, making it a valuable tool for both design and analysis of trapezoidal channels.

One-shot Halley-based explicit approximation

Presentation of the model

The one-shot Halley explicit approximation is an analytical, non-iterative model developed and adapted by the authors to evaluate the reduced normal flow depth in trapezoidal channels directly from the implicit governing relationship [Eq. (12)], while remaining distinct from the single-step Newton formulation already explored in this study. The model is built entirely from the mathematical structure and physical content of the governing equation and does not involve empirical fitting, tabulated coefficients, or calibration against numerical data.

The starting point of the model is the implicit equation that links the reduced normal flow depth z to the relative conductivity Q^* and the trapezoidal geometry, in which the unknown flow depth appears outside and inside nonlinear operators, notably square-root and cube-root terms. This structure reflects the hydraulic balance between relative conductivity, wetted geometry, and energy slope, but it also prevents a closed-form solution. The one-shot Halley approximation addresses this difficulty by combining asymptotic physical reasoning with a higher-order local linearization of the implicit operator.

From the physical viewpoint, the first building block is a reference depth obtained by identifying the dominant balance of the governing equation. When the relative conductivity is not vanishingly small, the term combining side slope and the square root of relative flow depth dominates the constant contribution inside the cube-root operator. This reflects the physical fact that, as flow increases, the wetted perimeter contribution associated with the inclined sidewalls governs the hydraulic resistance. Exploiting this dominance leads to a power-law relationship between the reduced flow depth and relative conductivity, with an exponent strictly derived from the structure of the governing equation and a coefficient that depends on the geometric parameter of the trapezoidal cross-section. To ensure physical consistency in the opposite limit of very small relative conductivity, this power-law scaling is augmented by an additive constant that reproduces the exact reduced normal flow depth obtained when Q^* tends to zero. The resulting expression provides a physically meaningful reference depth that simultaneously respects low-flow behavior and high-flow scaling.

From the mathematical viewpoint, the implicit governing equation is then recast as a scalar root-finding problem by defining a residual function whose zero corresponds exactly to the true reduced flow depth. Unlike purely asymptotic or fitted approximations, the one-shot Halley model exploits local information about the curvature of this residual function. In addition to the first derivative, which measures the local slope of the residual, the second derivative is evaluated analytically and retained in the formulation. This second derivative captures how rapidly the slope of the residual changes with flow depth, which is directly related to the nonlinear coupling introduced by the nested root operations in the governing equation.

The core of the model is a single Halley update applied to the physically derived reference depth. Halley's method is a third-order Householder scheme, meaning that it incorporates both first- and second-order information about the residual function. In practical terms, this allows the correction applied to the reference depth to account not only for the magnitude of the residual but also for the local curvature of the implicit operator. As a result, the update compensates more effectively for nonlinearity than a one-step Newton correction, especially in parameter regions where the governing equation is strongly curved, such as shallow side slopes or low reduced relative conductivity.

The intrinsic strength of the one-shot Halley approximation lies in this dual consistency. Globally, the reference depth is anchored in the correct physical scaling dictated by the governing equation and channel geometry. Locally, the Halley correction introduces higher-order accuracy by incorporating curvature information without resorting to iterative refinement. This combination yields an explicit approximation that is both robust and accurate over a wide range of relative conductivity and inclination angles, while maintaining a simple computational structure.

From an intrinsic mathematical standpoint, the model is self-contained and transparent: all quantities are obtained by direct evaluation of closed expressions derived from the governing equation itself. From a physical standpoint, the approximation respects limiting behaviors and dominant hydraulic mechanisms rather than forcing agreement through fitting. The resulting model therefore represents a natural higher-order extension of one-step Newton schemes, offering improved accuracy in a single evaluation while preserving simplicity, interpretability, and suitability for engineering applications.

It is emphasis to point out that "reference depth" does not mean a physical depth defined by an external criterion, such as critical depth, uniform-flow depth, or an empirical benchmark, nor does mean an arbitrary initial guess chosen for numerical convenience. In the context of the one-shot Halley model, the reference depth has a precise mathematical and physical meaning. It is an analytically constructed depth estimate obtained directly from the dominant balance of the implicit governing equation itself, before any corrective step is applied. In other words, it is the depth that the governing equation reduces to when its leading-order physical mechanisms are isolated and expressed explicitly.

From a mathematical point of view, the implicit governing equation contains several competing terms: a constant term, a geometry-dependent term involving the side slope, and nonlinear operators acting on the unknown flow depth. When the relative conductivity is not extremely small, one of these contributions clearly dominates inside the nonlinear operator. By formally extracting this dominant contribution and neglecting lower-order terms, the implicit equation collapses into a simpler algebraic balance that can be solved exactly. The solution of this reduced balance yields an explicit expression for the flow depth that captures the correct scaling of the true solution with respect to relative conductivity and channel geometry. This explicit solution is what is called the reference depth.

From a physical point of view, the reference depth represents the depth associated with the primary hydraulic control mechanism of the flow. In trapezoidal channels, as relative conductivity increases, the wetted geometry governed by the inclined sidewalls becomes the dominant contributor to the hydraulic resistance and energy balance, while secondary contributions become less influential. The reference depth embodies this dominant regime while still respecting the exact low-relative conductivity limit imposed by the governing equation. It is therefore physically meaningful, not arbitrary.

Crucially, the reference depth is not claimed to be the final solution. It is intentionally an approximation that is close to the true reduced normal flow depth over the entire parameter range, but it is not exact. Its role is to serve as a mathematically well-founded anchor point that already satisfies the correct asymptotic behavior and limiting properties of the system. Because it is constructed from the governing equation itself, it lies in the vicinity of the true solution for all admissible relative conductivities and inclination angles.

In the one-shot Halley approximation, this reference depth plays a central structural role: it is the depth at which the residual of the governing equation and its derivatives are evaluated. The Halley correction then uses local curvature information to transform this reference depth into a highly accurate final estimate in a single step. If the reference depth were poorly chosen or physically inconsistent, the one-shot correction would not be reliable across the full domain. The effectiveness of the Halley model therefore depends directly on the fact that the reference depth is a physically grounded, asymptotically consistent analytical approximation, not a numerical guess.

In short, the term “reference depth” denotes a physically meaningful, analytically derived baseline solution of the governing equation, which serves as the foundation upon which the one-shot Halley correction builds to achieve high accuracy without iteration.

Governing implicit equation written as a scalar root problem

First, let’s recall the following:

$$\omega = \left(Q^*\right)^{2/3} \tag{16}$$

$$s = \sqrt{1 + m^{-2}} \tag{17}$$

$$z = \frac{1}{4} + \omega\left[1 + s\left(2\sqrt{z} - 1\right)\right]^{1/3} \tag{18}$$

Let’s write the implicit governing Eq. (18) as a residual $f(z) = 0$ by moving all terms to one side; thus, it reads as follows:

$$f\left(z\right) = z - \frac{1}{4} - \omega\left[1 + s\left(2\sqrt{z} - 1\right)\right]^{1/3} \tag{114}$$

For compactness, let's define the following function:

$$u\left(z\right)=1+s\left(2\sqrt{z}-1\right) \tag{115}$$

Thus, Eq. (114) reduces to the following final form:

$$f\left(z\right)=z-\frac{1}{4}-\omega\left[u\left(z\right)\right]^{1/3} \tag{116}$$

Appropriate initial guess relationship

In this section, we adopt the following initial guess relationship developed in one the previous paragraphs:

$$z_0=\frac{1}{4}+\left(Q^*\right)^{4/5}\left(2s\right)^{2/5} \tag{30}$$

This is only a starting approximation; the final answer comes from the one-shot Halley correction that will be described in the next section.

Therefore, for $z = z_0$, Eq. (116) becomes:

$$f\left(z_0\right)=z_0-\frac{1}{4}-\omega\left[u\left(z_0\right)\right]^{1/3} \tag{116a}$$

where

$$u\left(z_0\right)$$

is given by Eq. (115) for $z = z_0$; it reads as follows:

$$u\left(z_0\right)=1+s\left(2\sqrt{z_0}-1\right) \tag{115a}$$

Exact first and second derivatives of $f\left(z\right)$

Differentiating $u(z)$ expressed by Eq. (115) yields what follows:

$$u'\left(z\right)=\frac{s}{\sqrt{z}} \tag{117}$$

Differentiating

$$\left[u\left(z\right)\right]^{1/3}$$

results in the following:

$$\frac{d}{dz}\left(u^{1/3}\right)=\frac{1}{3}u^{-2/3}u' \tag{118}$$

Substituting Eq. (117) into Eq. (118) yields the following:

$$\frac{d}{dz}\left(u^{1/3}\right)=\frac{1}{3}u^{-2/3}\frac{s}{\sqrt{z}} \tag{119}$$

Then, the first derivative of $f(z)$ expressed by Eq. (116) is as follows:

$$f'(z)=1-\omega\frac{1}{3}u^{-2/3}\frac{s}{\sqrt{z}} \tag{120}$$

Eq. (120) can be rewritten in the following form:

$$f'(z)=1-\frac{\omega s}{3\sqrt{z}}\left[u(z)\right]^{-2/3} \tag{121}$$

For $z=z_0$, Eq. (121) becomes as follows:

$$f'(z_0)=1-\frac{\omega s}{3\sqrt{z_0}}\left[u(z_0)\right]^{-2/3} \tag{121a}$$

Similarly, it is easy to show that the second derivative of $f(z)$, expressed by Eq. (116), can be written as follows:

$$f''(z)=-\frac{\omega s}{3}\left(-\frac{2s}{3\sqrt{z}}\left[u(z)\right]^{-5/3}-\frac{1}{2\sqrt{z^3}}\left[u(z)\right]^{-2/3}\right) \tag{122}$$

Therefore, for $z=z_0$, Eq. (122) is written as follows:

$$f''(z_0)=-\frac{\omega s}{3}\left(-\frac{2s}{3\sqrt{z_0}}\left[u(z_0)\right]^{-5/3}-\frac{1}{2\sqrt{z_0^3}}\left[u(z_0)\right]^{-2/3}\right) \tag{122a}$$

Halley's method for one update from z_0 allows us written the following final result:

$$z(\text{app}) = z_0 - \frac{2f(z_0)f'(z_0)}{2\left[f'(z_0)\right]^2 - f(z_0)f''(z_0)} \tag{123}$$

Eq. (123) defines a complete explicit model.

Distribution of the maximum relative deviation in z

Fig. 9 presents the maximum relative deviation, expressed in percent, between z predicted by the one-shot Halley-based explicit approximation and the corresponding exact solution given by Eq. (12), plotted as a function of the inclination angle α. Each point of the curve represents the worst deviation obtained for a given inclination angle when the relative conductivity Q^* is allowed to vary over its full domain, namely $Q^* \in [0.1, 4]$. In this sense, the curve is an envelope of relative errors and provides a conservative and global assessment of the accuracy of the Halley-based approximation with respect to α.

The figure has been deliberately restricted to the inclination angle range $10° \leq \alpha \leq 60°$, which corresponds to the recommended domain of application of the Halley model. Within this interval, the maximum deviation in z remains strictly below 0.1%, indicating a high level of accuracy for engineering purposes across the entire range of relative conductivity considered. The very low magnitude of the deviations, especially around intermediate inclination angles, confirms that the one-shot Halley formulation is capable of capturing the nonlinear behavior of the governing equation with excellent precision in this angular range.

The curve exhibits a smooth, continuous variation with α. Starting from $\alpha = 10°$, the maximum deviation is small and gradually decreases as α increases, reaching a minimum in the mid-range of angles ($\alpha \approx 36°$). Beyond this minimum, the deviation increases again as α approaches 60°, although it still remains below the 0.108% threshold. This behavior reflects the progressive change in the balance between geometric and hydraulic terms in the governing equation as the sidewalls become steeper, and it highlights the fact that the Halley-based correction remains effective as long as this balance does not become excessively skewed.

Inclination angles greater than 60° are not represented in the figure because, beyond this limit, the maximum deviation increases very rapidly. Numerical evaluation shows that the deviation grows almost exponentially for $\alpha > 60°$, exceeding 2% at $\alpha = 80°$. This sharp degradation in accuracy indicates that the one-shot Halley approximation is no longer reliable for very steep sidewall inclinations. Consequently, the model should be regarded as inaccurate outside the recommended range, and alternative formulations or iterative solutions should be used for α greater than 60°.

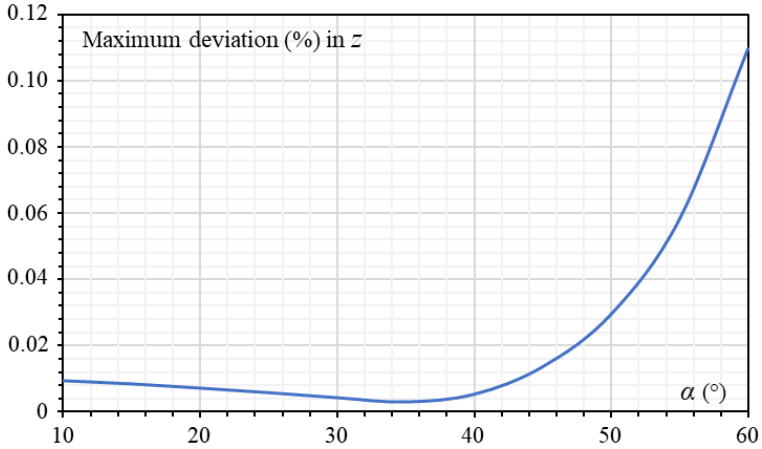

Figure 9: Maximum relative deviation (%) in z predicted by the one-shot Halley explicit approximation, expressed by Eq. (123), as a function of the inclination angle α within the full range $Q^* \in [0.1, 4]$ (recommended range: $\alpha \leq 60°$)

An important observation is that the general trend of the curve is practically the same as that previously obtained for the other explicit approximation models studied in the paper. In particular, the existence of a minimum deviation at intermediate angles and the rapid increase in error toward large inclination angles are consistent features shared by all models. This similarity confirms that the behavior is primarily dictated by the intrinsic structure of the governing equation and by the geometric effects associated with trapezoidal cross sections, rather than by the specific approximation technique itself. The figure therefore demonstrates that, while the one-shot Halley-based approximation offers excellent accuracy within a well-defined range, its limitations follow the same physical and mathematical constraints observed for some earlier models.

Secant-linearized quadratic approximation (SLQA) model

Presentation and positioning of the model

The Secant-Linearized Quadratic Approximation (SLQA) model is a new explicit approximate formulation developed by the authors for the implicit governing Eq. (12), recommended for the full inclination angle α range, typically $10° \leq \alpha \leq 80°$, and within the admissible relative conductivity range $0.1 \leq Q^* \leq 4$. It is distinct from all approximate models introduced in the paper, such as Taylor linearization, Halley-based models, MTQEA, etc., and is designed to provide: (1) High accuracy, (2) Strong mathematical consistency, (3) Explicit one-shot evaluation, (4) Simple algebraic structure, and (5) Clear physical interpretability.

The SLQA model relies on a two-point secant representation of the only nonlinear element in the transformed governing equation: the cube-root term originating from the trapezoidal geometry-hydraulic resistance coupling.

Governing equation structure and motivation

After transformation, it was shown earlier that the implicit Eq. (12) governing z may be written in a compact form, after defining the following functions:

$$\omega = \left(Q^*\right)^{2/3} \tag{16}$$

$$y = \sqrt{z}\,,\ y \geq 0 \tag{86}$$

$$x\left(y\right) = 1 + s\left(2y - 1\right) = 1 - s + 2s\,y \tag{88}$$

$$g\left(y\right) = \left[x\left(y\right)\right]^{1/3} \tag{89}$$

then Eq. (12), or Eq. (87), becomes as follows:

$$y^2 = \frac{1}{4} + \omega\, g\left(y\right) \tag{90}$$

Recall that, the transformed equation consists of: (1) a pure quadratic left-hand side, representing the flow depth-area scaling, and (2) a cube-root nonlinearity on the right-hand side represented by Eq. (89), encoding friction and geometry effects.

Thus, all the nonlinearity is concentrated in a single monotone function, while the argument of this function remains linear. This structure invites a targeted approximation strategy, where only the nonlinear component is approximated, while the original balance form is preserved.

Mathematical construction of the SLQA model

Instead of using a local Taylor expansion, as in first-order linearization, the SLQA model replaces the cube-root function $g(y)$ by a secant line constructed between the following two physically admissible points:

y_0 and y_1

such as writing the following with the “sec” denotes “secant”:

$$g\left(y\right) \approx g_{\sec}\left(y\right) = g_0 + k\left(y - y_0\right) \tag{124}$$

with

$$g_0 = g\left(y_0\right) \tag{125}$$

According to Eqs. (88) and (89), Eq. (125) can be written as follows:

$$g_0 = \left[1 + s\left(2y_0 - 1\right)\right]^{1/3} \tag{126}$$

$$k = \frac{g_1 - g_0}{y_1 - y_0} \tag{127}$$

$$g_1 = g\left(y_1\right) = \left[1 + s\left(2y_1 - 1\right)\right]^{1/3} \tag{128}$$

A secant (two-point) is a model because: (1) It captures global curvature effects, not just local slope, (2) It improves accuracy over a wide hydraulic range, (3) It preserves monotonicity and convexity properties of the cube-root function, and (3) It avoids explicit derivatives, improving robustness and simplicity.

In addition, because $x(y)$ expressed by Eq. (88) is linear, write it explicitly in the following generic form:

$$x\left(y\right) = ay + b \tag{129}$$

with constants a and b coming from the trapezoidal geometry and the "slope-intercept" form Eq. (88). One may write the following:

$$a = 2s \tag{130}$$

$$b = 1 - s \tag{131}$$

After in-depth investigation and computation, the authors recommend computing y_0 and y_1 with the following robust blends:

$$y_0 = \sqrt{\frac{1}{4} + \omega\left(b + \omega^{3/5}a^{6/5}\right)^{1/3}} \tag{132}$$

$$y_1 = \sqrt{\frac{1}{4} + \omega\left(ay_0 + b\right)^{1/3}} \tag{133}$$

That gives the user two good points for the secant line and typically makes the SLQA accurate over the overmentioned inclination angle range, provide that the relative conductivity Q^* is as $0.1 \leq Q^* \leq 4$.

Algebraic reduction to a quadratic equation

Substituting Eq. (124) into Eq. (90) yields the following:

$$y^2 = \frac{1}{4} + \omega\left[g_0 + k\left(y - y_0\right)\right] \tag{134}$$

Expanding the right-hand side of Eq. (134) results in what follows:

$$y^2 = \frac{1}{4} + \omega g_0 + \omega k y - \omega k y_0 \tag{135}$$

Bringing all terms to the left and rearranging, Eq. (135) can be written in the following form:

$$y^2 - \omega k y - \left(\frac{1}{4} + \omega g_0 - \omega k y_0\right) = 0 \tag{136}$$

Let's define the following constant:

$$C = \frac{1}{4} + \omega g_0 - \omega k y_0 \tag{137}$$

Then, Eq. (136) reduces to the following:

$$y^2 - \omega k y - C = 0 \tag{138}$$

Eq. (138) is an explicit quadratic in *y*.

Because

$$y = \sqrt{z}\,,\ y \geq 0 \tag{86}$$

the root which has a physical meaning is as follows

$$y = y(\text{app}) = \frac{k\omega + \sqrt{\left(k\omega\right)^2 + 4C}}{2} \tag{139}$$

According to Eq. (86), the sought following final result can be written:

$$z(\text{app}) = \left[\frac{k\omega + \sqrt{\left(k\omega\right)^2 + 4C}}{2}\right]^2 \tag{140}$$

Graphical distribution of the relative maximum deviation in z

Fig. 10 illustrates the variation of the maximum relative deviation (in percent) in z produced by the Secant-Linearized Quadratic Approximation (SLQA) model as a function of the inclination angle α of the trapezoidal channel. The horizontal axis represents the inclination angle α, expressed in degrees, spanning the interval $10° \leq \alpha \leq 80°$. The vertical axis shows the maximum deviation between the SLQA-predicted solution and the reference, numerically exact solution of the implicit governing Eq. (12), expressed in percent.

For each inclination angle, the plotted value corresponds to the worst-case (maximum) deviation observed over the admissible range of the relative conductivity, such as $0.1 \leq Q^* \leq 4$. The curve therefore represents a conservative accuracy envelope of the SLQA model with respect to α.

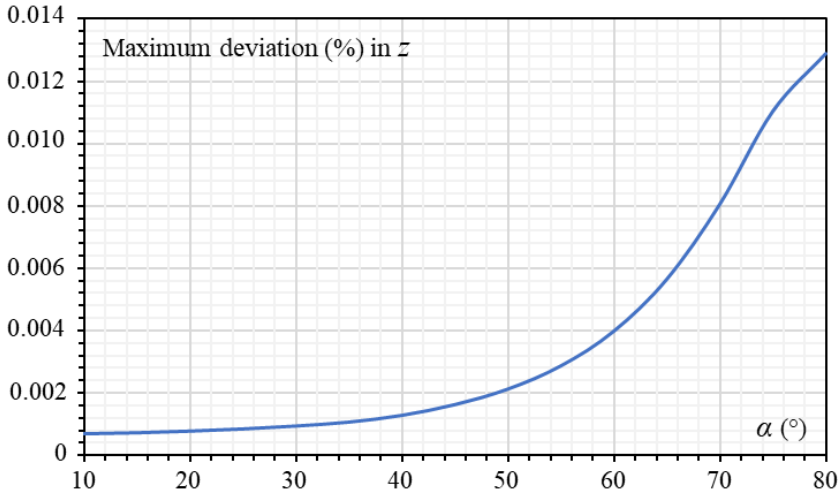

Figure 10: Maximum relative deviation (%) in z predicted by the SLQA model, expressed by Eq. (140), as a function of the inclination angle α within the full range $Q^* \in [0.1, 4]$

Fig. 10 reveals a smooth, monotonic increase of the deviation with increasing channel inclination. The most striking feature of the figure is the very low magnitude of the relative error across the entire displayed range: (1) The maximum deviation remains practically below 0.013% for $10° \leq \alpha \leq 80°$, (2) Even at the upper bound $\alpha = 80°$, the deviation does not exceed approximately 0.013%.
This confirms that the SLQA model is highly accurate over a wide range of geometries and flow conditions.

From a hydraulic-engineering perspective, such deviations are excellent, lying far below typical uncertainties associated with: (1) Manning's roughness coefficient, (2) discharge measurements, (3) geometric simplifications of real channels.

Thus, within the stated range of inclination angle, the SLQA model can be regarded as practically exact.

Fig. 10 shows a monotonic and mildly convex increase of the maximum deviation as α increases. This trend has a clear mathematical and physical explanation: (1) Increasing α alters the geometric contribution to the governing equation, which directly affects the linear argument of the cube-root term in the transformed formulation, (2) As α increases, the relative contribution of the slope-dependent term grows, enhancing the nonlinearity of the governing balance, and (3) Since the SLQA model relies on a secant linearization of the cube-root term, its accuracy naturally decreases when curvature effects become stronger.
Importantly, this loss of accuracy is gradual and controlled, not abrupt, indicating that the secant representation remains robust over the entire interval.

In the lower range of inclination angles, i.e., large side slope m, the maximum deviation is extremely small, typically of the order of 0.0005% to 0.001%, and the curve is almost flat, indicating very weak sensitivity of the SLQA relative error to α in this region. As a right interpretation, for small side slopes, wide or mildly trapezoidal channels, the governing equation is close to the very wide rectangular-channel limit. Consequently, the hydraulic radius varies slowly with depth, the linear argument ($a + by$) of the cube root is dominated by the term associated with the bottom width, and the cube-root nonlinearity is therefore weakly sensitive to y. In addition, Fig. 10 shows that the maximum SLQA deviation is extremely small, < 0.001%, and the curve is nearly flat. The SLQA approximation is almost exact in the wide-channel regime because the governing equation is only weakly nonlinear.

For intermediate inclination angles, typically $40° \leq \alpha \leq 60°$, which can be considered as a transition regime, the channel departs from the wide-rectangular limit, and the sidewalls contribute significantly to area and wetted perimeter. Consequently, the coupling between geometry and depth becomes stronger, and the cube-root nonlinearity becomes more sensitive to variations in y. In addition, one may observe the following behavior: a smooth and gradual increase in maximum deviation, and there is no instability or oscillation.
Thus, the secant-based SLQA model remains highly accurate but naturally reflects increased geometric nonlinearity.

For large inclination angles, typically $60° \leq \alpha \leq 80°$, corresponding to the case of rectangular-channel limit with walls tending to the vertical walls, the sidewalls are steep, approaching a true rectangular section, and, contrary to the wide-channel case, the hydraulic radius now varies more strongly with depth. Consequently, the cube-root argument becomes more sensitive to y, and the nonlinearity in the transformed equation is strongest. In addition, as it can be seen in Fig. 10, the maximum deviation increases more rapidly, and the maximum remains well below 0.014%. Although the rectangular-channel limit is a classical geometry, it is also a regime where depth sensitivity is higher. This explains the observed increase in the maximum deviation, while the SLQA model still performs exceptionally well.

The trend of the curve in Fig. 10 is physically consistent. The monotonic increase of the maximum deviation with α has a clear physical meaning: Small α: weak coupling, and minimal error, while large α: strong coupling, and slightly larger (but still negligible) relative error.

Fig. 10 confirms that the SLQA model is highly accurate within a wide and practically relevant range of inclination angles, namely: $\alpha \in [10°, 80°]$. This range is a well-defined domain of excellence.

In addition, most trapezoidal channels used in engineering practice, especially irrigation canals, drainage channels, and steep lined channels, fall comfortably within this angular interval.

The smoothness of the curve in Fig. 10 and the absence of oscillations or irregular behavior indicate that: (1) The SLQA model achieves sub-0.013% accuracy over a practically relevant range of channel inclinations, (2) The dependence of the relative error on α is smooth, predictable, and physically consistent, (3) The model is best classified as a highly accurate explicit approximation with a clearly bounded domain of validity, $\alpha \in [10°, 80°]$, $0.1 \leq Q^* \leq 4$, and (4) Within α =10°-80°, the SLQA model can be confidently used without iterative correction, even in precision-oriented hydraulic design.

A One-shot inverse quadratic interpolation approximation model (IQI)

Presentation of the model

The proposed model is an explicit, physics-consistent approximation developed adapted by the authors to determine the normal flow depth in trapezoidal open channels governed by the nonlinear implicit governing Eq. (12). Rather than attempting to force the governing equation into a purely explicit form, the model exploits the mathematical structure of the original hydraulic balance and combines it with a high-accuracy interpolation strategy.

The starting point of the development is the observation that the governing z relationship, [Eq. (12)], can be expressed as a fixed-point condition: the unknown parameter z appears simultaneously on both sides of the equation, linking hydraulic resistance, relative conductivity, and channel geometry through fractional power laws. This formulation is not an approximation; it is simply a rearrangement of the original physical law. Each evaluation of the right-hand side therefore represents a hydraulically admissible state in which gravity, friction, and geometry are fully balanced.

The model construction proceeds in the following three conceptually distinct stages.

First, a physically informed explicit estimate of z is introduced, i.e., initial guess z_0. This initial estimate is not arbitrary; it is derived from the asymptotic behavior of the governing equation and reflects the dominant influence of the relative conductivity and channel inclination. The relative conductivity appears through a power law consistent with uniform-flow scaling, while the geometric influence is introduced through a single compact parameter that reflects the side-slope configuration of the trapezoidal section.

This geometry parameter represents the combined effect of wall inclination on wetted perimeter and flow area. As a result, the initial depth estimate already satisfies the correct physical trends for both shallow and moderately deep flows.

Second, the governing hydraulic relationship itself is used as an operator to generate two additional z states from the initial estimate, i.e., z_1 and z_2. Each application of this operator corresponds to enforcing the uniform-flow balance using the previously obtained z. Importantly, these evaluations are not iterations in the classical sense; they are direct substitutions into the original hydraulic law [Eq. (12)]. Consequently, the three resulting z values can be interpreted as three physically meaningful flow configurations, all consistent with the same relative conductivity and channel geometry but differing in their proximity to the exact equilibrium state.

Third, these three z states are combined using an inverse quadratic interpolation framework applied to the residual of the governing relationship. The residual measures how far a given z is from satisfying the hydraulic balance exactly. Values of z associated with smaller residuals are naturally closer to the true z value. The interpolation process constructs a local quadratic representation of the inverse relationship between the residual and z, allowing the equilibrium point to be extracted directly without further iteration. The resulting expression for z is fully explicit and requires no derivatives, tuning coefficients, or convergence criteria.

From a physical standpoint, the final approximation can be viewed as a weighted synthesis of three hydraulically admissible flow states. The weights are not empirical; they are determined solely by how strongly each candidate z violates the governing balance. This ensures that the approximation remains anchored to the underlying physics rather than to curve fitting or regression.

The strength of the model lies in its ability to capture the nonlinear interaction between relative conductivity and geometry with very high accuracy while retaining the simplicity of an explicit formula. Because the model is built directly on the governing hydraulic law, it preserves correct monotonicity, scaling behavior, and asymptotic limits. At the same time, the use of inverse quadratic interpolation provides an accuracy that is typically associated with advanced iterative methods, but herein it is achieved in a single, closed-form evaluation.

In practical terms, the model offers a robust compromise between purely explicit formulas and iterative numerical solvers. It requires only a small number of straightforward algebraic evaluations, yet its accuracy approaches that of exact numerical solutions. This makes it particularly well suited for engineering applications where computational efficiency, transparency, and physical consistency are equally important.

In short, the IQI proposed model is a semi-analytical, physics-based approximation that transforms the solution of an implicit uniform-flow equation into a single explicit calculation. It is mathematically grounded, physically interpretable, and computationally efficient, providing a reliable tool for normal-flow depth estimation in trapezoidal open channels across a wide range of flow and geometric conditions.

Relationships used

Below are the relationships used in the proposed model, which are not new equations since they were developed earlier.

The implicit governing Eq. (12) is recalled as follows:

$$z = \frac{1}{4} + \left(Q^*\right)^{2/3}\left[1 + \left(2\sqrt{z} - 1\right)\sqrt{1 + m^{-2}}\right]^{1/3} \qquad (12)$$

The initial guess relationship, expressed by Eq. (30), is recalled as follows:

$$z_0 = \frac{1}{4} + \left(Q^*\right)^{4/5}\left(2s\right)^{2/5} \qquad (30)$$

Define the following mapping

$$\Phi : \mathbb{R}^+ \to \mathbb{R}^+$$

by the right-hand side of Eq. (12); it reads as follows:

$$\Phi\left(z\right) = \frac{1}{4} + \left(Q^*\right)^{2/3}\left[1 + \left(2\sqrt{z} - 1\right)\sqrt{1 + m^{-2}}\right]^{1/3} \qquad (141)$$

Then the governing implicit equation is exactly as follows:

$$z = \Phi\left(z\right) \qquad (142)$$

This is the same fixed-point structure used in a previous section, expressed by Eq. (47), when it introduces the following repeated substitution:

$$z_{n+1} = \Phi\left(z_n\right) \qquad (47)$$

Let's define the following residual function:

$$f\left(z\right) = \Phi\left(z\right) - z \qquad (143)$$

Then solving Eq. (142) is equivalent to the following:

$$f\left(z\right) = 0 \qquad (144)$$

Generate two additional points

Compute two more points by direct substitution into Eq. (47); then, the following is written:

$$z_1 = \Phi\left(z_0\right) \qquad (145)$$

$$z_2 = \Phi\left(z_1\right) \tag{146}$$

Recall that the function Φ is governed by Eq. (141).

This produces the following three abscissas

$$\left\{z_0,\, z_1,\, z_2\right\} \tag{147}$$

used in the IQI approximator.

Compute residuals at those three points

Using Eq. (142), the following can be derived:

$$f_0 = f\left(z_0\right) = \Phi\left(z_0\right) - z_0 \tag{148}$$

$$f_1 = f\left(z_1\right) = \Phi\left(z_1\right) - z_1 \tag{149}$$

$$f_2 = f\left(z_2\right) = \Phi\left(z_2\right) - z_2 \tag{150}$$

Because of Eqs. (145) and (146), two of these can be written directly as the following differences:

$$f_0 = z_1 - z_0 \tag{151}$$

$$f_1 = z_2 - z_1 \tag{152}$$

Model formulation

First, for clarity, define the following three IQI weights:

$$A_0 = \frac{f_1 f_2}{\left(f_0 - f_1\right)\left(f_0 - f_2\right)} \tag{153}$$

$$A_1 = \frac{f_0 f_2}{\left(f_1 - f_0\right)\left(f_1 - f_2\right)} \tag{154}$$

$$A_2 = \frac{f_0 f_1}{\left(f_2 - f_0\right)\left(f_2 - f_1\right)} \tag{155}$$

The one-shot IQI approximation given the sought z (app) is as follows:

$$z(\text{app}) = A_0 z_0 + A_1 z_1 + A_2 z_2 \tag{156}$$

It can be rigorously demonstrated that the weighting coefficients obey the following identity:

$$A_0 + A_1 + A_2 = 1 \tag{157}$$

Distribution of the relative maximum deviation (%) in z

Fig. 11 illustrates the distribution of the maximum relative deviation (in percent) in z produced by the proposed IQI-based approximation model. The results are obtained by systematically varying the relative conductivity Q^* over its full practical range $[0.1, 4]$ and the channel sidewall inclination angle α between 10° and 80°. For each inclination angle, the reported deviation corresponds to the maximum relative error observed over the entire range of relative conductivity. The figure thus represents a worst-case accuracy assessment of the model with respect to geometric inclination.

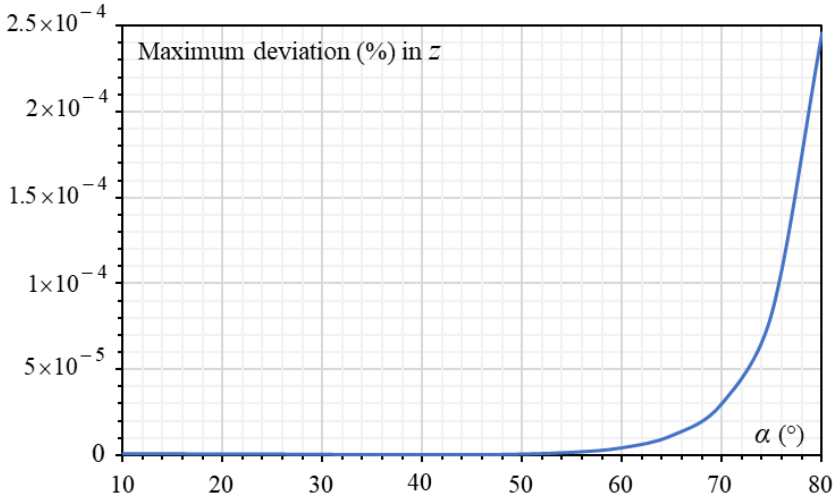

Figure 11: Maximum deviation (%) in z produced by the IQI model expressed by Eq. (156) for $0.1 \leq Q^* \leq 4$

The figure provides a comprehensive and conservative evaluation of the accuracy of the IQI model by reporting the maximum deviation in z for each inclination angle. By maximizing the relative error over the full conductivity range at each angle, the analysis ensures that the displayed curve reflects the most unfavorable conditions for the model, rather than average or locally optimal behavior.

A key observation is that the maximum deviation remains negligible over a wide range of inclination angles, namely from 10° up to approximately 60°. In this interval, the

maximum relative deviation is effectively indistinguishable from zero on the scale of the figure, demonstrating that the IQI model is quasi-exact throughout this domain. This result is particularly significant, as it encompasses the inclination angles most commonly encountered in practical engineering applications of trapezoidal open channels.

From a physical perspective, this remarkable accuracy can be attributed to the moderate influence of channel geometry on the nonlinear structure of the governing equation within this angular range. For small to intermediate inclinations, the geometric parameter entering the model varies smoothly, and the fixed-point operator retains a weakly nonlinear character. Under such conditions, the inverse quadratic interpolation mechanism is able to reconstruct the equilibrium z with near machine-precision accuracy using only three hydraulically admissible states.

Beyond approximately 60°, the figure shows a progressive increase in the maximum deviation, culminating near the upper bound of 80°. This trend reflects the increasing dominance of geometric effects as the sidewalls approach a near-vertical configuration. In this regime, the nonlinearity of the governing relationship becomes more pronounced, and small variations in z induce relatively larger changes in the hydraulic balance. Despite this increase, it is important to emphasize that the maximum relative deviation remains extremely small, even at the highest inclination angles considered.

Broadly speaking, Fig. 11 demonstrates that the IQI model combines exceptional robustness with very high accuracy across a broad parameter space. Its quasi-exact performance for inclination angles up to 60°, together with its controlled and smoothly varying relative error beyond this limit, confirms the model's suitability for both standard engineering applications and more extreme geometric configurations. The absence of erratic behavior or abrupt loss of accuracy further highlights the numerical stability and physical consistency of the proposed approach.

Propagation of the relative deviation in z into the rough-reference model relative flow depth η_R

Once z is obtained using one on the previous studied models, the sought relative normal depth, or the aspect ratio, in the rough reference model, is recovered using Eq. (11a) which is recalled as follows:

$$\eta_R = \left(\sqrt{z} - \frac{1}{2}\right) m^{-1} \tag{11a}$$

Eq. (11a) can be rewritten simply as follows:

$$\eta_R = \frac{\sqrt{z} - \frac{1}{2}}{m} \tag{11b}$$

Let's define the following notations:

$$z(\text{exact})$$

is the exact value of z provided by the exact implicit governing Eq. (12), and

$$z(\text{app})$$

is the z value delivered by one of the approximate models developed earlier.

Let's also define the relative deviation in z, produced by the model, as follows:

$$\varepsilon_z(\%) = 100 \times \frac{\left| z(\text{app}) - z(\text{exact}) \right|}{z(\text{exact})} \tag{124}$$

Thus, from Eq. (124), the following can be derived:

$$z(\text{app}) = z(\text{exact})\left(1 + \varepsilon_z\right) \tag{125}$$

Then:

$$\sqrt{z(\text{app})} = \sqrt{z(\text{exact})}\sqrt{1 + \varepsilon_z} \tag{126}$$

Using Eq. (11b), the corresponding values of η_R are as follows:

$$\eta_R(\text{exact}) = \frac{\sqrt{z(\text{exact})} - \frac{1}{2}}{m} \tag{127}$$

$$\eta_R(\text{app}) = \frac{\sqrt{z(\text{app})} - \frac{1}{2}}{m} \tag{128}$$

Substituting Eq. (126) into Eq. (128) yield the following:

$$\eta_R(\text{app}) = \frac{\sqrt{z(\text{exact})}\sqrt{1 + \varepsilon_z} - \frac{1}{2}}{m} \tag{129}$$

Hence the exact relative deviation in η_R can be written as follows:

$$\varepsilon_\eta(\%) = 100 \times \frac{\eta_R(\text{app}) - \eta_R(\text{exact})}{\eta_R(\text{exact})} \tag{130}$$

Using Eqs. (127) and (129), and rearranging, yields the following final relationship:

$$\varepsilon_\eta\,(\%) = \frac{\sqrt{z\,(\text{exact})}}{\sqrt{z\,(\text{exact})} - \dfrac{1}{2}}\left(\sqrt{1 + \varepsilon_z} - 1\right) \tag{131}$$

This is the exact propagation law, no approximation yet: it shows that the relative error in η_R is governed by a square-root transformation of the relative deviation in z, and it is amplified by the following factor

$$\frac{\sqrt{z\,(\text{exact})}}{\sqrt{z\,(\text{exact})} - \dfrac{1}{2}} \tag{132}$$

The above factor is entirely determined by the hydraulic state through z(exact) and is independent of the side slope m because m cancels out when forming the relative error in η_R.

Case of small relative deviations ε_z

For the common case of small relative deviations in z, that can be expressed by the following inequality:

$$\left|\,\varepsilon_z\,\right| \ll 1 \tag{133}$$

one may use the following first-order expansion:

$$\sqrt{1 + \varepsilon_z} \approx 1 + \varepsilon_z / 2 \tag{134}$$

Substituting this result into the exact Eq. (131) gives the following first-order relative error propagation:

$$\varepsilon_\eta\,(\%) = \frac{\sqrt{z\,(\text{exact})}\left(1 + \varepsilon_z / 2 - 1\right)}{\sqrt{z\,(\text{exact})} - \dfrac{1}{2}} \tag{135}$$

which can be reduced to the following:

$$\varepsilon_\eta\,(\%) = \frac{\sqrt{z\,(\text{exact})}}{2\left(\sqrt{z\,(\text{exact})} - \dfrac{1}{2}\right)}\varepsilon_z \tag{136}$$

Therefore, if deviations are reported in percent, the same proportionality applies as following:

$$\text{Deviation}\,(\%)\,\text{in}\,\eta_{\mathrm{R}} \approx \frac{\sqrt{z\left(\text{exact}\right)}}{2\left(\sqrt{z\left(\text{exact}\right)}-\frac{1}{2}\right)} \times \text{Deviation}\,(\%)\,\text{in}\,z \tag{137}$$

It is useful to recall that Eq. (137) is valid for small relative deviations in z. It can be state that the amplification factor is expressed as follows:

$$\mathrm{A}_f = \frac{\sqrt{z\left(\text{exact}\right)}}{2\left(\sqrt{z\left(\text{exact}\right)}-\frac{1}{2}\right)} \tag{138}$$

It is a local sensitivity multiplier.

Case of large relative deviations ε_z

Mathematically, this case can be translated as follows:

$$\varepsilon_z \to \infty \tag{139}$$

This case is generally not of practical interest when assessing or interpreting an approximate mathematical model governing z. This case means that the approximate model produces a value of z that deviates strongly from the exact solution, and the approximation is not valid in that regime. This is not a subtle mathematical artifact, it is a failure of the model. It is also means that the model does not represent the physics correctly, error-propagation results become irrelevant, and any "interesting" asymptotic behavior is mathematically correct but physically meaningless.

Key interpretation

The interpretation of error propagation must be restricted to the domain in which the approximate model governing z is valid. In practical terms, this means that only situations where the relative deviation in z remains small are of interest. When the deviation in z becomes large, the corresponding model is no longer accurate and must be excluded from consideration. Such cases have no practical relevance in hydraulic analysis, since an inaccurate prediction of z inevitably leads to unreliable estimates of all derived quantities.

Within the valid regime of small deviations in z, the way errors propagate from z to the relative aspect ratio depends primarily on the level of the flow depth. When the flow depth is large, the transformation linking z to the relative aspect ratio, Eq. (11a) or (11b), naturally attenuates errors. In this regime, a small relative deviation in z produces an even smaller relative deviation in the aspect ratio, indicating that the latter is less sensitive to modelling inaccuracies. This behavior provides a form of robustness, since moderate errors in z have a limited impact on the aspect ratio when the flow is relatively deep.

By contrast, when the flow depth approaches its lower admissible limit, the system becomes highly sensitive. This lower limit corresponds to the minimum physically meaningful flow depth for which the formulation remains valid, that is, the threshold below which the geometrical representation of the flow section degenerates and the aspect ratio tends toward zero. Near this limit, even very small deviations in z may result in comparatively large relative errors in the aspect ratio. This increased sensitivity is inherent to the geometry and the definition of the variables, and does not reflect a deficiency of the propagation analysis itself.

As a concluding remark, the propagation of modelling errors from z to the relative aspect ratio is well behaved and weak over most of the practical range of flow depths. The aspect ratio is generally less sensitive than z to modelling inaccuracies when the flow depth is moderate to large. Pronounced sensitivity arises only in very shallow flow conditions, close to the lower admissible limit of the flow depth, where extra care is required. As long as the approximate model for z remains accurate and is used within its intended domain of validity, the resulting predictions of the relative aspect ratio remain reliable.

Numerical example

Now, consider the following numerical example based on Halley-model. Let's adopt the following data:

$$\alpha = 45^\circ \text{ , } Q^* = 2$$

According to the implicit governing Eq. (12), the following is derived:

$$z(\text{exact}) = 2.842107126$$

The Halley model-based Eq. (123) gives the following approximate result:

$$z(\text{app}) = 2.84185583$$

Therefore, the relative deviation in z, produced by the model, is given by Eq. (124) as follows:

$$\varepsilon_z(\%) = 100 \times \frac{\left| z(\text{app}) - z(\text{exact}) \right|}{z(\text{exact})} \tag{124}$$

The final result being as follows:

$$\varepsilon_z(\%) = 0.00884202$$

Thus, applying the general Eq. (131) yields the following final result:

$$\varepsilon_\eta(\%) = 0.00627124$$

Thus, it can be observed that the relative deviation in z does not amplify the relative deviation in η_R; on the contrary, it leads to a reduction of this deviation for the example considered.

When applying the approximate Eq. (137) derived for small relative deviations in z, practically the same result is obtained, since:

$$\varepsilon_\eta(\%) = 0.00628507$$

In this case, the amplification factor [Eq. (138)] is as follows:

$$A_f = \frac{\sqrt{z(\text{exact})}}{2\left(\sqrt{z(\text{exact})} - \frac{1}{2}\right)} = 0.71081835$$

Thus, the amplification factor is less than unity, which explains why the relative error in η_R is mitigated, or reduced.

Amplification factor

Amplification of relative deviations in normal-flow depth computations

An important and often underestimated aspect of the normal-flow depth problem in trapezoidal open channels is the amplification of numerical deviations when transferring results from the reduced normal flow depth parameter z to the physically meaningful flow depth. Even when the relative error in the reduced variable remains small, the corresponding error in the actual relative normal flow depth η_R, or normal flow depth ratio, expressed by Eqs. (11a) or (11b), may be significantly larger. This phenomenon is not accidental and does not depend on the numerical method employed; it is an intrinsic consequence of the mathematical structure of the governing relationship expressed by Eq. (12).

The reduced normal depth z used in the analysis is not a linear measure of flow depth, but rather a quadratic representation derived from it. Because of this nonlinear transformation, small deviations in the reduced parameter z, produced by one of the approximate models developed herein, inevitably propagate in a non-uniform way when converted back to the physical relative normal flow depth. The mapping between the two quantities becomes particularly sensitive near the lower bound of admissible flow, where the reduced normal flow depth z approaches its minimum value. In this regime, even a very small variation in the reduced parameter induces a comparatively large variation in the relative normal flow depth itself.

This sensitivity results in what can be described as an amplification mechanism: the relative deviation in the normal-flow depth exceeds the relative deviation initially present in the reduced variable z. The amplification is strongest for shallow flows, corresponding to low relative conductivity, where the hydraulic system operates close to its limiting

configuration. Under such conditions, the flow geometry reacts sharply to incremental changes in flow depth, and any numerical imprecision is magnified by the nonlinear response of the governing formulation. As the flow becomes deeper and the reduced depth increases, this amplification weakens progressively, and the system behaves in a more regular and less sensitive manner.

From a physical standpoint, this amplification reflects the fact that shallow flows are inherently more sensitive to perturbations. Small changes in flow depth significantly affect the wetted perimeter, hydraulic radius, and energy dissipation mechanisms, which in turn have a pronounced impact on the flow conditions. Consequently, the mathematical amplification of deviations mirrors a genuine hydraulic sensitivity rather than a purely numerical artifact.

The existence of this amplification factor has important practical implications. It explains why approximate solutions that appear reasonably accurate when judged solely on the reduced depth parameter may nonetheless produce unacceptable errors in the computed normal-flow depth. It also clarifies why extremely small deviations in the reduced variable are required to ensure reliable hydraulic predictions, especially for low to moderate flow rates and gently inclined sidewalls. In this context, the stringent accuracy observed in well-designed fixed-point and accelerated solution schemes is not excessive; it is a necessary condition imposed by the physics of the problem.

Moreover, the amplification factor provides a unifying interpretation of the error patterns observed across different approximation techniques. Regardless of whether a method is iterative, semi-analytical, or fully explicit, the dependence of the error on channel geometry and relative conductivity follows the same qualitative trend. This confirms that the amplification phenomenon is dictated by the governing equation itself, not by the choice of solution strategy.

Positive and negative amplification of relative deviations

However, in the analysis of approximate models for normal-flow flow depth, amplification of relative deviations should not be regarded exclusively as a detrimental effect. While classical sensitivity analysis often highlights positive amplification, where errors produced by an approximate model are magnified when transferred to the physical flow depth, there also exists a complementary and equally important phenomenon: negative amplification, more appropriately described as attenuation of relative deviations.

Positive amplification corresponds to situations in which the mathematical transformation linking the reduced variable to the physical flow depth intensifies any discrepancy introduced by the model. In this case, a small relative deviation in the reduced parameter results in a larger relative deviation in the flow depth itself. This behavior is most pronounced near hydraulic lower bounds, where the governing relationship becomes highly sensitive. Positive amplification therefore exposes numerical imperfections and places strict demands on the accuracy of approximate formulations.

In contrast, negative amplification arises when the structure of the governing transformation counteracts the model's deviation, leading to a reduction of the relative error as it propagates toward the physical variable. Under such circumstances, the transformation acts as a stabilizing filter: the computed flow depth deviates less from the exact value than the reduced variable on which it is based. This attenuation effect does not imply that the model is intrinsically exact in the reduced variable; rather, it indicates that the nonlinear mapping redistributes errors in a favorable manner.

The existence of negative amplification is not contradictory to the theory of error propagation. It reflects the fact that amplification factors depend not only on the magnitude of the deviation but also on the local curvature and scaling of the transformation between variables. Depending on the operating point in the parameter space, the transformation may either enhance or dampen deviations. As a result, the same approximate model can exhibit positive amplification in one hydraulic regime and negative amplification in another.

This dual behavior explains observations often reported in numerical studies where certain explicit or semi-explicit approximations produce normal flow depth estimates that are more accurate than might be expected from their reduced-variable performance alone. In such cases, attenuation masks part of the model's intrinsic error and yields a flow depth estimate that is closer to the exact solution. While this effect may appear beneficial, it should not be misinterpreted as unconditional robustness. Attenuation is conditional and regime-dependent; a model benefiting from negative amplification at moderate flow depths may suffer from strong positive amplification at lower depths.

Therefore, amplification factors, whether positive or negative, should be interpreted as diagnostic indicators rather than absolute measures of model quality. A good approximation is not simply one that benefits from attenuation at specific points, but one that maintains controlled and predictable behavior across the full range of application. From an engineering standpoint, both amplification and attenuation must be acknowledged, as they govern the reliability of the flow depth prediction under varying hydraulic conditions.

In short, the amplification of relative deviations represents a fundamental feature of the normal-flow depth problem in open-channels, such as trapezoidal channels. It highlights the need for high-precision computation of the reduced normal flow depth and justifies the development of robust and carefully controlled approximation methods. Recognizing and accounting for this amplification is essential for ensuring that numerical solutions translate into physically accurate and practically reliable estimates of normal flow depth. In addition, positive amplification reveals sensitivity and exposes model inaccuracies, while negative amplification temporarily conceals them by attenuating errors. A comprehensive assessment of approximation methods must recognize both effects and avoid conclusions based on isolated cases. Understanding the sign and magnitude of amplification is essential for evaluating not only the numerical accuracy of a model, but also its hydraulic credibility and practical reliability.

Complementary discussion on the role of amplification in model assessment

The recognition of both positive and negative amplification mechanisms calls for a careful and nuanced interpretation of numerical results obtained from approximate normal-flow depth models. In particular, the apparent performance of a model cannot be evaluated solely on the basis of isolated error values or single test cases. An approximation that benefits from attenuation effects under specific hydraulic conditions may appear highly accurate, while the same formulation may exhibit significant deficiencies when applied outside that limited range.

From a methodological perspective, the existence of attenuation should not be confused with intrinsic numerical robustness. Negative amplification may temporarily compensate for modelling inaccuracies in the reduced variable, but this compensation remains contingent upon the local behavior of the governing transformation. Consequently, attenuation does not eliminate the underlying error; it merely alters its manifestation in the physical variable. This distinction is essential when assessing the general applicability and reliability of explicit or semi-explicit formulations.

The dual nature of amplification also provides a clear explanation for the sometimes-divergent conclusions reported in the literature regarding the comparative performance of approximation schemes. Differences in channel geometry, relative conductivity, or flow regime may shift the balance between amplification and attenuation, leading to contrasting error patterns even for the same numerical method. This reinforces the need for systematic testing over a wide range of hydraulic conditions, rather than reliance on a narrow subset of favorable cases.

In practical engineering applications, awareness of amplification effects is particularly important because design decisions are ultimately based on the physical flow depth. When positive amplification dominates, small computational inaccuracies may translate into unacceptable design errors, especially for shallow flows and near-threshold regimes. Conversely, when attenuation is present, the apparent accuracy of a method should be interpreted with caution, as favorable error reduction may not persist under different operating conditions.

Ultimately, the amplification factor serves as a valuable interpretative tool that links numerical accuracy to hydraulic sensitivity. By explicitly acknowledging the possibility of both amplification and attenuation, analysts can better discriminate between genuinely robust approximation methods and those whose apparent performance depends strongly on regime-dependent error redistribution. This understanding strengthens the theoretical foundation of normal-flow depth modelling and contributes to more reliable and transparent evaluation of approximate solutions in open-channel hydraulics.

Amplification factor for small relative deviations $\mathcal{E}_Z$ [Eq. (138)]

Interpretation and significance

In the context of small relative deviations in the reduced normal depth z, Eq. (138) introduces an amplification factor that plays a central role in understanding how numerical errors propagate toward the physically meaningful relative normal-flow depth. This factor establishes a direct proportionality between the relative deviation in the reduced variable z and the resulting relative deviation in the relative flow depth ratio η_R. It is therefore not a numerical artifact linked to a particular approximation, but an intrinsic feature of the governing transformation itself.

The amplification factor depends solely on the hydraulic state through the exact value of the reduced depth. Its value reflects the local sensitivity of the normal-flow depth formulation to perturbations in the reduced variable. When this factor exceeds unity, relative deviations in the reduced flow depth are magnified in the corresponding flow depth ratio, indicating positive amplification. In contrast, when the factor is less than unity, the transformation attenuates errors, leading to what is commonly referred to as negative amplification.

The amplification factor defined by Eq. (138) therefore provides a powerful diagnostic tool for assessing approximation methods. It clarifies why relative deviations in the reduced normal flow depth must be interpreted with caution and why error evaluation should always be conducted in relation to the physical quantity of interest. Positive and negative amplification are complementary manifestations of the same nonlinear transformation, and neither should be ignored when judging model reliability.

In other words, Eq. (138) formalizes the notion that error propagation in normal-flow depth computations is governed as much by the mathematical structure of the problem as by the numerical quality of the approximation. Recognizing the sign and magnitude of the amplification factor is essential for ensuring that computed flow depths are not only numerically accurate, but also hydraulically meaningful and practically reliable.

Variation of the amplification factor in the case of small relative deviations $\mathcal{E}_Z$ [Eq. (138)]

Fig. 12 illustrates the evolution of the amplification factor defined by Eq. (138), along with the implicit governing Eq. (12), as a function of the relative conductivity Q^* over the interval from 0.1 to 4. The amplification factor is evaluated for the two extreme sidewall inclination angles considered in the study, namely 10° (orange curve) and 80° (blue curve). These two curves bound the entire family of intermediate inclination angles; the latter are not shown because their corresponding curves are practically superposed and therefore visually indistinguishable at the scale of the figure.

The horizontal green dashed line marks the threshold value separating amplification from attenuation. This line represents the upper limit of the negative amplification zone, that

is, the limit below which the relative deviation in the relative normal flow depth is reduced with respect to the relative deviation in the reduced depth parameter z. Above this limit, the amplification factor exceeds unity and the error in the relative normal flow depth is magnified.

Fig. 12 therefore provides a compact and synthetic representation of how the transfer of relative deviations from the reduced variable to the normal flow depth depends jointly on hydraulic conditions, through Q^*, and channel geometry, through the inclination angle.

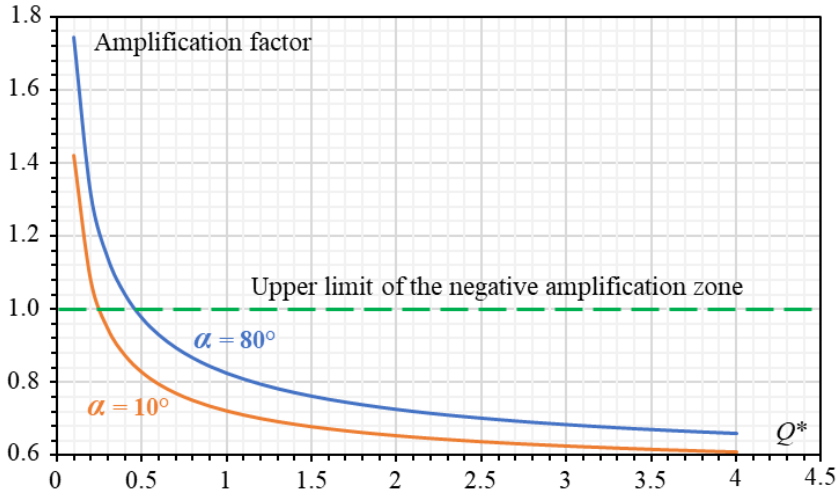

Figure 12: Variation in the amplification factor computed according to Eq. (138), along with Eq. (12), with respect to the relative conductivity, and for the inclination angles α = 10° and 80°

Several important and physically meaningful conclusions can be drawn from Fig. 12.

First, the amplification factor decreases monotonically as the relative conductivity increases, regardless of the inclination angle. This confirms that error propagation is most critical in low-conductivity regimes, corresponding to shallow and hydraulically sensitive flows. As the flow becomes more energetic and deeper, the system progressively loses sensitivity, and the transformation from the reduced variable to the normal depth becomes more stable.

In Fig. 12, the amplification factor quantifies how a relative deviation already present in the reduced depth variable is transmitted to the relative normal flow depth. Saying that propagation is most critical refers to the situation in which this transmission mechanism is both highly sensitive and potentially harmful to accuracy.

More specifically, propagation becomes critical when small modelling errors in the reduced variable are no longer innocuous, but instead have a disproportionately large impact on the physically meaningful normal flow depth. In this regime, even a carefully constructed approximation may lead to unacceptable errors in the final hydraulic quantity if the reduced variable is not computed with very high accuracy.

In Fig. 12, this criticality occurs in the low relative conductivity domain, where the amplification factor rises sharply. Physically, this domain corresponds to shallow or near-threshold flows, in which the hydraulic configuration is inherently sensitive. Under such conditions, the transformation linking the reduced variable to the relative normal flow depth behaves like a magnifier: tiny inaccuracies are expanded rather than absorbed.

Thus, the term "most critical", used previously, does not simply mean "largest amplification." It means that: (1) the hydraulic system reacts strongly to perturbations, (2) numerical relative errors cease to be safely transferable, and (3) the reliability of approximate solutions becomes highly dependent on accuracy.

In addition, in the critical propagation regime, error control becomes decisive since approximations that are adequate elsewhere may fail, apparent small discrepancies in intermediate variables can undermine the final relative normal flow depth prediction, and the numerical stability of solution methods must be particularly strong.

This explains why the paper emphasizes small-deviation assumptions, convergence acceleration, and high-accuracy formulations, especially when dealing with shallow flows. The governing relationship itself imposes this requirement; it is not an artifact of any specific approximation technique.

In contrast, when the amplification factor falls below the threshold shown in Fig. 12, i.e., green dashed line, the propagation becomes non-critical, so that: deviations are attenuated rather than magnified, the transformation acts as a stabilizing filter, and approximate models appear more robust and forgiving.

Thus, as a concise statement, by stating that "propagation is most critical," this meant that there exists a hydraulic regime in which the mapping from reduced normal flow depth to physical relative flow depth is so sensitive that error transmission becomes the dominant limitation on model reliability. Fig. 12 identifies this regime and explains why accuracy requirements are most stringent precisely where the flow is hydraulically most delicate.

Second, for a very large portion of the investigated domain, the amplification factor remains below the threshold value indicated by the green dashed line. This means that, in this region, the transformation induces attenuation of relative deviations: the error in the computed relative normal flow depth is smaller than the error produced by the model in the reduced flow depth parameter z. This "negative" amplification explains why certain approximate models may appear particularly effective when evaluated directly in terms of normal flow depth, even if their reduced-variable accuracy is more modest.

Third, the effect of channel geometry, although present, is clearly secondary. The curves corresponding to the extreme inclination angles frame a narrow band, within which all intermediate cases lie. This shows that the amplification behavior is governed primarily by the hydraulic state, via the relative conductivity, rather than by the sidewall inclination. Geometry modulates the amplification factor, but it does not fundamentally alter its trend or its order of magnitude.

Fourth, the amplification factor becomes significantly larger than unity only in the low-Q^* range. This identifies a critical hydraulic zone in which even very small deviations in

the reduced normal flow depth z may produce noticeable errors in the actual relative normal flow depth. In practical terms, this justifies the high level of accuracy required from numerical or approximate solutions in shallow-flow conditions and explains why stringent convergence criteria are necessary in this regime.

Finally, Fig. 12 highlights the dual nature of amplification. “Positive” amplification exposes model inaccuracies by magnifying them, whereas “negative” amplification may partially mask these inaccuracies by attenuating their effect on the computed relative normal depth. This duality reinforces the idea that model assessment cannot rely on isolated cases: an approximation that performs well thanks to attenuation in one regime may perform poorly in another where amplification prevails.

Overall, Fig. 12 provides a clear and unified visual interpretation of the role played by the amplification factor introduced in Eq. (138). It confirms that error propagation in normal-flow depth computations is strongly regime-dependent, dominated by the hydraulic state, and only weakly affected by geometry. Most importantly, it explains why both error magnification and error attenuation are natural and inevitable consequences of the nonlinear structure of the governing formulation.

Amplification factor, sensitivity, and elasticity: Conceptual relationships and distinctions

The amplification factor, sensitivity, and elasticity are closely related concepts that all describe how a system responds to variations in its controlling parameters (Achour et al., 2025). Despite this common objective, they differ in both their conceptual scope and their practical interpretation. Clarifying their similarities and differences is essential for properly understanding the behavior of normal-flow depth models and for avoiding ambiguous interpretations of numerical results.

Sensitivity is a local concept that quantifies how strongly an output variable responds to a small change in an input parameter. It expresses the immediate reaction of the system in absolute or relative terms and is typically evaluated at a specific operating point. Sensitivity answers the question of how much the solution changes when a parameter is perturbed slightly, without accounting for how this change propagates through subsequent transformations or variable redefinitions.

Elasticity refines this notion by focusing specifically on relative variations. It measures the proportional response of an output variable to a proportional change in an input variable. Elasticity is dimensionless and scale-independent, which makes it particularly attractive for comparing the influence of different parameters or for evaluating the responsiveness of a model across ranges of magnitude. However, elasticity remains tied to the direct relationship between an input and an output variable and does not, by itself, account for the structural effects of variable transformations.

The amplification factor differs fundamentally from both sensitivity and elasticity in that it does not describe how an output responds to a change in an input, but rather how an error or deviation already present in one variable is transformed when transferred to

another variable. In other words, sensitivity and elasticity address cause-effect relationships, while the amplification factor addresses error propagation. It quantifies how deviations are redistributed by the mathematical structure of the governing formulation, independently of the origin of those deviations.

Despite this distinction, there is a clear conceptual bridge between these notions. The amplification factor may be viewed as a form of derived sensitivity, not with respect to an external parameter, but with respect to a change of variables. It reflects the local sensitivity of one variable to another and thus depends on the curvature and scaling of the transformation linking them. In this sense, the amplification factor inherits some of the same local and state-dependent characteristics as sensitivity and elasticity, while applying them to the propagation of deviations rather than to parameter influence.

Another important distinction lies in interpretation. Sensitivity and elasticity are often used to rank parameters according to their influence on model outputs or to assess robustness to uncertainty in input data. The amplification factor, by contrast, is primarily a diagnostic tool that assesses the reliability of approximate solutions. It reveals whether errors produced in an intermediate or reduced variable will be magnified or attenuated in the final physical quantity of interest. Its sign and magnitude therefore carry direct implications for the practical usefulness of a model.

At the same time, the amplification factor shares with elasticity the ability to reveal regime-dependent behavior. Just as elasticity may vary significantly across operating conditions, the amplification factor may change in magnitude and even in qualitative effect, shifting from attenuation to amplification as hydraulic conditions evolve. This reinforces the idea that neither sensitivity, elasticity, nor amplification should be interpreted as global constants; all are local descriptors whose relevance depends on the state of the system.

Overall, sensitivity, elasticity, and amplification address different but complementary aspects of system behavior. Sensitivity describes how outputs react to parameter changes, elasticity measures proportional responsiveness, and the amplification factor characterizes how deviations propagate through variable transformations. The amplification factor can be viewed as a bridge between numerical accuracy and physical relevance, linking model error to hydraulic response in a way that sensitivity and elasticity alone cannot capture. Recognizing their interrelationship provides a more complete framework for analyzing model performance and for ensuring that numerical accuracy translates into meaningful and reliable physical predictions.

Existence of a universal minimum in approximation relative error around $\alpha \approx 45°$

A remarkable and recurrent observation emerging from the present study is that, with the sole exception of the fixed-point method (Fig. 2), all approximation strategies investigated, namely the controlled analytical explicit model (Fig. 3), the Aitken-Steffensen accelerated scheme (Fig. 4), the one-step Newton method (Fig. 5), and the derivative-free secant approximation (Fig. 7), produce maximum relative error curves that systematically pass through a minimum located near an inclination angle of $\alpha \approx 45°$. This

convergence of minima across fundamentally different methods is neither accidental nor method-dependent; rather, it reflects a deep geometric and mathematical property of the governing implicit Eq. (12) itself.

The implicit governing Eq. (12) is structured around a nonlinear operator combining square-root and cube-root dependencies, in which the channel geometry enters exclusively through the following inclination-dependent parameter:

$$s = \sqrt{1 + m^{-2}} = \sqrt{1 + \tan^2 \alpha} \tag{17}$$

This parameter simultaneously influences: (1) the growth rate of the wetted area, (2) the evolution of the wetted perimeter, and (3) the sensitivity of the Eq. (12) defines a nonlinear mapping that associates any tentative value of the reduced flow depth z with a new value obtained through combined square-root and cube-root transformations involving the sidewall inclination."

At $\alpha = 45°$, the geometry of the trapezoidal section attains a unique symmetry: horizontal and vertical projections of the sidewalls are equal, implying $m = 1$ and, thus, a balanced contribution of area expansion and perimeter growth. In this configuration, the nonlinear operator governing Eq. (12), such as $\sqrt{z}$, becomes locally least curved with respect to z. Consequently, the following can be written: (1) higher-order nonlinear terms are weakest, (2) the local linearization error is minimized, and (3) In the vicinity of $\alpha \approx 45°$, the nonlinear governing equation exhibits minimal sensitivity to variations in the reduced flow depth z, which explains why approximation errors are smallest in this range. In other words, the governing equation is least sensitive to flow depth variations near $\alpha \approx 45°$, which naturally minimizes approximation errors.

Any approximation technique, whether analytical (Fig. 3), extrapolative (Fig. 4), or predictive (Figs. 5 and 7), benefits maximally from this structural regularity. Hence, all approximation errors naturally attain a minimum near $\alpha \approx 45°$, independent of the specific numerical machinery employed.

From a hydraulic standpoint, $\alpha \approx 45°$ corresponds to a trapezoidal geometry where the channel achieves an optimal compromise between conveyance efficiency and geometric stability, allowing writing the following: (1) small variations in flow depth produce proportional and smooth changes in both cross-sectional area and wetted perimeter; (2) the hydraulic diameter evolves gently with depth; and (3) resistance effects are distributed uniformly between bed and sidewalls.

As a result, the flow system is least sensitive to geometric perturbations, and the reduced normal flow depth z responds smoothly to changes in conductivity. Any approximation capturing the dominant balance of the governing equation will therefore perform best in this regime, regardless of its analytical complexity.

However, the fixed-point Halley methods are an exception. As for the Halley-model, the fixed-point method does not aim to approximate the solution directly; instead, its deviation measure reflects the contractive strength of the iteration, not the truncation error of an explicit model. The deviation between successive iterates is controlled primarily by

the derivative of the fixed-point map, which does not vanish at $\alpha = 45°$. Therefore, Fig. 2 does not exhibit a pronounced minimum at that angle, even though the exact solution itself remains exceptionally stable there. This distinction highlights an important methodological nuance: iteration-based convergence metrics and approximation-based accuracy metrics do not respond identically to geometry, even though both are governed by the same governing equation.

From the consistent behavior observed in Figs. 3, 4, 5, and 7, the following strong and general statement may be formulated:

Corollary (Geometric optimality of $\alpha \approx 45°$)

For the implicit Darcy-Weisbach-RMM normal-flow depth governing equation in trapezoidal channels, the sidewall inclination $\alpha \approx 45°$ constitutes a geometrically optimal configuration in which the nonlinear operator is maximally regular. Consequently, all physically consistent one-shot approximations of the equation attain their highest accuracy in the vicinity of this angle, independently of the analytical or numerical technique employed.

This corollary is not an empirical observation but a direct manifestation of the intrinsic symmetry and smoothness properties of the governing equation. It provides both a theoretical explanation of the observed behavior and a practical guideline for hydraulic design and modelling.

From an engineering perspective, this result carries a clear message: trapezoidal channels with sidewall inclinations around 45° are not only hydraulically efficient but also numerically optimal. In this range, explicit and semi-explicit approximations yield near-exact results with minimal computational effort. Even when steeper or flatter geometries are required for structural or site constraints, the deviation trends remain smooth and predictable, confirming the robustness of the proposed solution framework.

The distinction between hydraulic economy and numerical optimality: the roles of 45° and 60° sidewall inclinations

The apparent contradiction between the statement that "sidewall inclinations around 45° are numerically optimal" and the classical assertion that "a 60° angle is the most economical" arises from a fundamental difference in the criteria being optimized. These two angles do not compete within the same framework; rather, they correspond to distinct performance concepts that must be clearly separated to remove any ambiguity.

The meaning of "most economical" at 60°

In classical open-channel hydraulics, the statement that a trapezoidal channel with sidewall inclination $\alpha = 60°$, i.e. $m \approx 0.577$, is the most economical refers to a purely geometric-hydraulic optimization problem. Specifically, this angle emerges when minimizing the wetted perimeter for a given cross-sectional area, or equivalently, when

maximizing the hydraulic radius under fixed conveyance constraints. This criterion is rooted in: (1) minimizing frictional resistance, (2) maximizing flow capacity per unit wetted perimeter, and (3) achieving material efficiency in excavation or lining.
In this sense, the 60° configuration is "economical" from a construction and energy-loss standpoint, independent of any analytical or numerical considerations. It is a static, geometry-driven result derived from calculus applied to cross-sectional shape.

What is meant by "numerical optimality" at 45°

By contrast, the observation that approximation relative errors reach a minimum around $\alpha \approx 45°$ is not a statement about hydraulic efficiency or construction economy. It is a statement about the mathematical structure of the implicit governing equation for normal flow depth and how this structure responds to geometry when approximate solution methods are employed.

"Numerical optimality" herein means that: (1) the nonlinear operator embedded in the governing equation is least sensitive to perturbations in depth, (2) higher-order nonlinear terms, associated with square-root and cube-root dependencies, are naturally balanced, and (3) the local curvature of the operator with respect to the unknown z is minimized.

At $\alpha = 45°$, the trapezoidal section exhibits a geometric symmetry: horizontal and vertical contributions of the sidewalls are equal. This symmetry produces a mathematical regularization of the governing equation that is especially favorable to explicit and semi-explicit approximations. Consequently, many different approximation methods, despite their distinct formulations, achieve their smallest relative errors near this angle.
This has nothing to do with minimizing wetted perimeter or construction cost; it is purely a consequence of relative error propagation and nonlinear sensitivity.

Why the two optima do not coincide and should not

There is no theoretical reason why the angle that minimizes wetted perimeter ($\approx 60°$), and the angle that minimizes approximation relative error in solving an implicit equation ($\approx 45°$), should coincide. They arise from different objective functions as shown in the following comparative Table 3.

Table 3: Comparison of the hydraulic and numerical characteristics of trapezoidal sidewall inclination Angles 45° and 60°

Aspect	60° angle	45° angle
Optimization criterion	Hydraulic radius/wetted perimeter	Error sensitivity of nonlinear operator
Nature	Physical-geometric	Mathematical-numerical
Depends on	Cross-section geometry only	Governing equation + approximation method
Relevance	Design and construction economy	Accuracy and robustness of analytical/numerical solutions

Thus, comparing 45° and 60° without distinguishing these objectives leads to a category error.

How to distinguish their "performance" unambiguously

The ambiguity is resolved once performance is explicitly qualified: If performance means hydraulic efficiency or construction economy, then the 60° angle remains the correct and well-established result of classical theory; If performance means robustness and accuracy of approximate flow depth computations, especially when using explicit or semi-explicit formulations, then the 45° angle emerges as numerically optimal.

In practical applications, the two considerations coexist but play different roles, as: channel geometry may be chosen near 60° for economic or structural reasons, while designers and analysts can be confident that approximation methods will remain most accurate near 45° and degrade smoothly as the angle departs from that value.

Importantly, the observed increase in approximation relative error as α approaches 60° or beyond does not invalidate the economic optimality of that angle; it merely signals that nonlinear sensitivity is higher and that more refined numerical treatment, e.g. additional Newton steps, may be warranted.

A clarifying statement to avoid future ambiguity

A strong and unambiguous formulation is therefore the following:

Clarifying statement

An inclination angle close to 60° emerges as hydraulically optimal, as it provides a favorable geometric configuration that minimizes the wetted perimeter while enhancing conveyance efficiency for a given cross-sectional capacity. By contrast, an inclination angle near 45° proves to be numerically optimal, since it reduces the intrinsic nonlinearity and sensitivity of the implicit governing equation for normal flow depth, thereby minimizing the relative deviations associated with explicit and semi-explicit approximation schemes. These two optimal configurations correspond to fundamentally distinct performance criteria, one rooted in hydraulic efficiency and geometric economy, the other in numerical stability and computational robustness, and therefore should not be expected to coincide.

Concluding sentence

The results corresponding to inclination angles of 45° and 60° are not contradictory but complementary. Each reflects a distinct dimension of optimality in trapezoidal channel design: the former emphasizes numerical stability and analytical robustness, while the latter captures hydraulic-geometric efficiency and structural economy. Taken together, these findings demonstrate that optimality in open-channel hydraulics is inherently multi-criteria, encompassing physical performance, construction considerations, and

computational reliability. Recognizing this distinction enables engineers and researchers to make deliberate, well-informed decisions without conflating geometric hydraulic efficiency with numerical convenience."

Main results of the monograph

The fundamental contribution of this monograph lies in demonstrating that the normal flow depth in trapezoidal open channels can be determined within a fully coherent physical framework that avoids prescribing empirical resistance coefficients as fixed parameters. By recasting the uniform-flow problem through the Darcy-Weisbach equation integrated with the Rough Model Method (RMM), the analysis eliminates the implicit circularity inherent in conventional Manning and Chézy formulations. In traditional practice, resistance coefficients are introduced as known inputs, despite the fact that they vary with hydraulic conditions, conditions that depend directly on the very normal depth being sought. The Darcy-Weisbach-RMM formulation resolves this inconsistency by expressing the governing relationship exclusively in terms of directly measurable physical and geometric variables, including discharge, channel geometry, bed slope, kinematic viscosity, and boundary roughness.

At the heart of the proposed framework lies the formulation of a dimensionless implicit equation governing a reduced normal-flow depth parameter, which constitutes the central mathematical structure of the method. This equation encapsulates the hydraulic problem in a compact, self-sufficient form, independent of empirically prescribed resistance coefficients. To solve it, the study develops an enhanced fixed-point procedure distinguished by the introduction of a hydraulically informed adaptive initial estimate, replacing the traditionally adopted constant starting value. This tailored initialization significantly improves convergence behavior by positioning the first iterate in close proximity to the true solution over wide ranges of relative conductivity and channel inclination. As a result, the iterative process reaches engineering-grade accuracy after only one to a few updates, maintaining strong numerical stability even for steep trapezoidal geometries.

A further significant outcome of the study is the demonstration that the proposed fixed-point formulation exhibits not merely convergence, but pronounced contractive behavior throughout the investigated hydraulic domain. This property is established quantitatively by examining the relative differences between successive iterates, notably between the third and fourth updates of the reduced normal flow depth variable. For instance, in the representative configuration with a sidewall inclination angle $\alpha = 45°$, the maximum discrepancy between these successive iterates across the following conductivity full range $0.1 \leq Q^* \leq 4$ is approximately 0.0065%, indicating extremely rapid attenuation of the iteration error and near-immediate stabilization of the solution. More generally, the analysis reveals a systematic dependence of the residual magnitude on wall inclination: deviations remain negligible for moderate angles and increase gradually as the sidewalls approach steep configurations, yet consistently remain far below customary hydraulic design uncertainties. This behavior confirms the method's numerical robustness and reliability across a wide spectrum of trapezoidal geometries.

Beyond the development of efficient iterative procedures, one of the monograph's most practically significant contributions lies in the construction of explicit, one-shot analytical approximations capable of reproducing the implicit Darcy-Weisbach-RMM solution with remarkable fidelity. These formulations eliminate the need for iterative looping, convergence criteria, or user-defined stopping thresholds, thereby providing a fully deterministic computational tool for the direct estimation of normal flow depth. Such characteristics are particularly advantageous in engineering contexts where transparency, speed, and simplicity are essential, including manual verification calculations, spreadsheet-based workflows, preliminary design sizing, and embedded implementations in hydraulic software modules.
Importantly, these explicit approximations are not empirical curve-fits or heuristic simplifications; rather, they are derived from controlled mathematical treatment of the original implicit governing relationship. As a result, they preserve consistency with the underlying Darcy-Weisbach-RMM physical framework and maintain close agreement with the reference implicit solution across the full investigated domain of relative conductivity and wall inclination. Engineers are thus provided with rapid computational alternatives that retain theoretical integrity and avoid the conceptual shortcomings associated with prescribing fixed Manning or Chézy coefficients.

An additional conceptual contribution of the study lies in its amplification-factor interpretation of numerical accuracy. The analysis demonstrates that deviations occurring in the reduced dimensionless variable governing the implicit equation do not propagate uniformly to the physically meaningful normal flow depth. Owing to the nonlinear transformation that links the reduced parameter to the actual flow depth, certain hydraulic regimes attenuate numerical deviations, whereas others amplify them. Consequently, the true measure of approximation quality is not the residual error in the intermediate variable itself, but its propagated impact on the computed normal flow depth.
By framing the discussion in terms of deviation transfer and sensitivity amplification, the study explicitly connects numerical error to the hydraulic responsiveness of the channel geometry. This perspective clarifies under which geometric and conductivity conditions explicit approximations remain safely within engineering tolerances, and under which configurations iterative refinement is advisable. In doing so, it transforms error analysis from a purely numerical exercise into a hydraulically meaningful assessment of solution reliability.

The monograph further highlights an inclination angle of $\alpha = 45°$ as a particularly advantageous configuration from the standpoint of numerical stability and computational robustness. Around this geometry, the implicit governing equation exhibits comparatively reduced nonlinear sensitivity, which translates into stronger contraction of the associated fixed-point mapping and faster attenuation of successive iteration errors. As a consequence, fixed-point convergence is especially rapid, residual deviations are minimal, and the derived explicit and semi-explicit approximation methods attain their highest accuracy within the investigated parameter range. From a computational perspective, this inclination therefore represents a well-balanced configuration, offering enhanced predictability and stability of the normal-flow depth solution across varying hydraulic conditions.

However, the study also underscores a critical practical distinction: numerical optimality, characterized by minimal nonlinearity and error propagation, is not synonymous with hydraulic optimality, which is typically defined in terms of geometric efficiency, conveyance performance, or wetted-perimeter minimization. These two criteria arise from fundamentally different considerations and should not be expected to coincide. Recognizing this distinction enables engineers to select sidewall inclinations based on clearly identified design objectives, avoiding the conflation of computational convenience with hydraulic performance.

CONCLUSION

From an engineering standpoint, this work provides a practical and reliable alternative to traditional Manning-based normal depth calculations. By eliminating empirically assumed resistance coefficients and replacing them with a physically consistent Darcy-Weisbach-RMM formulation, the method ensures that all required inputs, discharge, geometry, slope, roughness, and viscosity, are directly measurable and hydraulically meaningful.

For routine design applications, the enhanced fixed-point method with adaptive initial guess converges rapidly and predictably across wide ranges of discharge and channel geometry. In most practical cases, three iterations are sufficient to reach engineering accuracy. When rapid evaluation is required, such as in spreadsheet tools, embedded calculators, or parametric optimization studies, the explicit analytical approximation and the Aitken-Steffensen one-shot scheme provide highly accurate results without iterative looping.

The study also identifies trapezoidal sections with sidewall inclination around 45° as particularly favorable for both hydraulic stability and numerical robustness. In this configuration, nonlinear amplification effects are minimized, resulting in superior predictive performance.

Overall, the presented framework offers the following practical advantages: no need to assume empirical resistance coefficients, high numerical stability across shallow and steep trapezoidal geometries, explicit alternatives for rapid computation, extremely small deviations compared to fully converged solutions, and straightforward implementation in hydraulic design software.

For designers and hydraulic engineers, the proposed methodology provides a consistent, efficient, and scientifically sound basis for normal depth determination in trapezoidal channels, suitable for both detailed analysis and routine engineering design.

Declaration of competing interest

The authors declare that they have no known competing financial interests or personal relationships that could influence the work reported in this article.

REFERENCES

ACHOUR B. (2014). Computation of Normal Depth in Trapezoidal Open Channel Using the Rough Model Method, Advanced Materials Research, Trans Tech Publications Ltd, Vols. 955-959, pp. 3231-3237.

ACHOUR B., AMARA L. (2020a). Manning's roughness coefficient in a trapezoidal-shaped channel, Technical Note, Larhyss Journal, No 44, pp. 89-96.

ACHOUR B., AMARA L. (2020b). Proper relationship of Manning's coefficient in a partially filled circular pipe, Larhyss Journal, No 42, pp. 107-119.

ACHOUR B., BEDJAOUI A. (2006). Discussion of "Exact solutions for normal depth problem", Journal of Hydraulic Research, International Association of Hydraulic Research (IAHR), Vol. 44, Issue 5, pp. 715-717.

ACHOUR B., BEDJAOUI A. (2012). Turbulent Pipe-flow Computation Using the Rough Model Method (RMM), Journal of Civil Engineering and Science (JCES), Vol. 1, Issue 1, pp. 36-41.

ACHOUR B., AMARA L., KULKARNI K.H. (2025). Exact theoretical rating law for sharp-crested elliptic, semi-elliptic, and circular weirs, Larhyss Journal, No 64, pp. 199-324.

AMARA L., ACHOUR B. (2023). Delta-perturbation expansion for the normal flow depth problem in rectangular channels, Larhyss Journal, No 55, pp. 231-241.

CHOW V.T. (1973). Open channel hydraulics, McGraw Hill Editions, New York, NY, USA.

COLEBROOK C.F. (1939). Turbulent Flow in Pipes, with Particular Reference to the Transition Region between the Smooth and Rough Pipe Laws, Journal of the Institution of Civil Engineers (ICE), London United Kingdom, UK, Vol. 11, pp. 133-156.

DARCY H. (1854). On experimental research concerning the movement of water in pipes, Proceedings of the Meetings of the Academy of Sciences, Paris, France, Vol. 38, pp. 1109-1121. (In French)

FRENCH R.H. (1986). Open Channel Hydraulics, McGraw Hill Editions, New York, NY, USA.

LAKEHAL M, ACHOUR B. (2017). New approach for the normal depth computation in a trapezoidal open channel using the rough model method, Larhyss Journal, No 32, pp. 269-284.

LAKEHAL M., ACHOUR B. (2014). Calculation of the normal depth in an egg-shaped conduit using the rough model method, Larhyss Journal, No 19, pp. 101-113. (In French)

SEHTAL S., ACHOUR B. (2023). Normal depth computation in a vaulted rectangular channel using the rough model method (RMM), Larhyss Journal, No 54, pp. 193-216.

SINNIGER R.O., HAGER W.H. (1989). Hydraulic Structures, Editions Romandes Polytechnic Press, Switzerland. (In French)

SWAMEE P.K. (1994). Normal-depth equations for irrigation canals, Journal of Irrigation and Drainage Engineering, American Society of Civil Engineers (ASCE), Vol. 120, Issue 5, pp. 942-948.

SWAMEE P.K., RATHIE P.N. (2004). Exact solutions for normal depth problem, Journal of Hydraulic Research, International Association of Hydraulic Research (IAHR), Vol. 42, Issue 5, pp. 541-547.

VATANKHAH A.R. (2013). Explicit solutions for critical and normal depths in trapezoidal and parabolic open channels, Ain Shams Engineering Journal, Vol. 4, Issue 1, pp. 17-23.